Aerosol properties over the Indo-Gangetic Plain: A mesoscale perspective from the TIGERZ experiment

David M. Giles,[1,2,3] Brent N. Holben,[2] Sachchida N. Tripathi,[4] Thomas F. Eck,[2,5] W. Wayne Newcomb,[6] Ilya Slutsker,[1,2] Russell R. Dickerson,[3] Anne M. Thompson,[7] Shana Mattoo,[8] Sheng-Hsiang Wang,[2,3,9] Remesh P. Singh,[10] Aliaksandr Sinyuk,[1,2] and Joel S. Schafer[1,2]

Received 14 February 2011; revised 16 June 2011; accepted 23 June 2011; published 20 September 2011.

[1] High aerosol loading over the northern Indian subcontinent can result in poor air quality leading to human health consequences and climate perturbations. The international 2008 TIGERZ experiment intensive operational period (IOP) was conducted in the Indo-Gangetic Plain (IGP) around the industrial city of Kanpur (26.51°N, 80.23°E), India, during the premonsoon (April–June). Aerosol Robotic Network (AERONET) Sun photometers performed frequent measurements of aerosol properties at temporary sites distributed within an area covering ~50 km^2 around Kanpur to characterize pollution and dust in a region where complex aerosol mixtures and semi-bright surface effects complicate satellite retrieval algorithms. TIGERZ IOP Sun photometers quantified aerosol optical depth (AOD) increases up to ~0.10 within and downwind of the city, with urban emissions accounting for ~10–20% of the IGP aerosol loading on deployment days. TIGERZ IOP area-averaged volume size distribution and single scattering albedo retrievals indicated spatially homogeneous, uniformly sized, spectrally absorbing pollution and dust particles. Aerosol absorption and size relationships were used to categorize black carbon and dust as dominant absorbers and to identify a third category in which both black carbon and dust dominate absorption. Moderate Resolution Imaging Spectroradiometer (MODIS) AOD retrievals with the lowest quality assurance (QA ≥ 0) flags were biased high with respect to TIGERZ IOP area-averaged measurements. MODIS AOD retrievals with QA ≥ 0 had moderate correlation (R^2 = 0.52–0.69) with the Kanpur AERONET site, whereas retrievals with QA > 0 were limited in number. Mesoscale-distributed Sun photometers quantified temporal and spatial variability of aerosol properties, and these results were used to validate satellite retrievals.

Citation: Giles, D. M., et al. (2011), Aerosol properties over the Indo-Gangetic Plain: A mesoscale perspective from the TIGERZ experiment, *J. Geophys. Res.*, *116*, D18203, doi:10.1029/2011JD015809.

1. Introduction

[2] The TIGERZ experiment (2008–2011) was conducted by the NASA Aerosol Robotic Network (AERONET) project within the Indo-Gangetic Plain (IGP) in northern India located south of the Himalayan foothills, and the intensive operational period (IOP) occurred during the 2008 premonsoon (April–June). The TIGERZ IOP foci included the spatial and temporal characterization of columnar aerosol optical, microphysical, and absorption properties; the identification of aerosol particle type mixtures; and the validation of remotely sensed aerosol properties from satellites. Data collection and analysis involved scientists, engineers, and graduate students from 20 institutions in Europe, India, and North America.

[3] Aerosol conditions over the IGP during the premonsoon are affected by locally generated and regionally transported aerosol particles such as fine mode pollution containing secondary organic carbon (OC) and black carbon (BC) from urban and industrial sources as well as dust mainly from nearby arid agricultural lands and the Thar Desert [*Middleton*, 1986; *Littmann*, 1991; *Chu et al.*, 2003; *Dey et al.*, 2004; *Singh et al.*, 2004; *Prasad et al.*, 2007;

[1]Sigma Space Corporation, Lanham, Maryland, USA.
[2]Goddard Space Flight Center, NASA, Greenbelt, Maryland, USA.
[3]University of Maryland, College Park, Maryland, USA.
[4]Indian Institute of Technology, Department of Civil Engineering, Kanpur, India.
[5]Universities Space Research Association, Columbia, Maryland, USA.
[6]Deceased 18 December 2008.
[7]Pennsylvania State University, University Park, Pennsylvania, USA.
[8]Science Systems and Applications, Inc., Lanham, Maryland, USA.
[9]Department of Atmospheric Sciences, National Central University, Chung-Li, Taiwan.
[10]School of Earth and Environmental Sciences, Chapman University, Orange, California, USA.

Copyright 2011 by the American Geophysical Union.
0148-0227/11/2011JD015809

Remer et al., 2008; *Gautam et al.*, 2009; *Arola et al.*, 2011]. These aerosol particles challenge remote sensing algorithms for ground-based sensors due to the combined temporal and spatial variability of dust resembling thin cirrus clouds, and algorithms for space-based sensors due to assumed aerosol absorption models and semi-bright land surface during the premonsoon. General circulation models have simulated shifts in the monsoon circulation due in part to high aerosol loading and radiative effects of BC and dust particles over the IGP. The Elevated Heat Pump (EHP) hypothesis proposed by *Lau et al.* [2006] and *Lau and Kim* [2006] was explored by the 2007–2011 Joint Aerosol–Monsoon Experiment (JAMEX) activities to further understand aerosol-monsoon interactions [*Lau et al.*, 2008]. Within this context, the AERONET project initiated the TIGERZ experiment to measure aerosol properties at sites spanning the IGP in 2008. Of note, the TIGERZ experiment (i.e., "tigers") was a larger follow-on effort to the smaller Cloud-Aerosol Lidar and Infrared Pathfinder Satellite Observation (CALIPSO) and Twilight Zone (CATZ) experiment (i.e., "cats") held in the Baltimore/Washington, D. C., region during the summer of 2007 [*McPherson et al.*, 2010]. Although the TIGERZ experiment had several components, one element was to establish up to seven temporary sites near Kanpur, India (26.51°N, 80.23°E) located ~300 km south of the Himalayan foothills. In addition to the long-term monitoring AERONET site at the Indian Institute of Technology (IIT) Kanpur, these TIGERZ sites provided the framework to quantify the spatial and temporal variability of columnar aerosol optical depth (AOD, τ), volume size distribution, and single scattering albedo (SSA). Long-term AERONET Kanpur data and TIGERZ results were examined to identify BC and dust particle mixtures from aerosol size, shape, and absorption properties. Last, the TIGERZ mesoscale deployment data set was utilized for validation of aerosol retrievals from satellite (e.g., Moderate Resolution Imaging Spectroradiometer (MODIS)).

2. Instrumentation, Study Region, and Techniques

2.1. Instrumentation

[4] Direct Sun and sky radiance measurements were conducted using the fully autonomous robotic Cimel Electronique CE-318 model radiometers (referred to as Cimels hereafter) deployed by the NASA AERONET project. The measurement protocols, calibration techniques, and data processing have been described by *Holben et al.* [1998] and *Eck et al.* [1999, 2005], but important details are provided here. The AERONET Cimels have a full field of view of 1.2° and use two common filter configurations: standard 8-filter (340, 380, 440, 500, 675, 870, 940, 1020 nm) and extended 9-filter (standard plus 1640 nm). Field instruments were inter-calibrated against AERONET reference Cimels, which are calibrated at Mauna Loa by Langley analyses [*Shaw* 1980, 1983; *Eck et al.*, 2005]. Columnar AOD, columnar water vapor (CWV) in centimeters, and almucantar retrievals utilized AERONET Version 2 algorithms and data quality criteria [*Smirnov et al.*, 2000; *Dubovik et al.*, 2000, 2006; *Holben et al.*, 2006]. However, due to the deviation from standard AERONET protocol (i.e., ~30-s rather than ~15-min intervals), temporary site Level 1.5 AOD data were manually cloud screened and quality assured using the detailed field logs. The accuracy of AERONET field Cimels varies spectrally from ±0.01 to ±0.02 for measured columnar AOD with higher errors in the ultraviolet channels [*Holben et al.*, 1998; *Eck et al.*, 1999], is within 10% for CWV retrievals [*Schmid et al.*, 2001; *Smirnov et al.*, 2004], and is typically less than 5% for calibrated sky radiances [*Holben et al.*, 1998]. In addition, the manually operated Solar Light Microtops II Sun photometers (referred to as Microtops hereafter) performed direct Sun measurements [*Morys et al.*, 2001]. The Microtops had varying sets of five filters utilizing the nominal wavelengths 440, 675, 870, and 940 with either 340 nm or 500 nm. Microtops data were collected using measurement and data processing protocols established by the Maritime Aerosol Network (MAN) component of AERONET [*Smirnov et al.*, 2009]. An artifact of the Microtops ~2° full field of view is to allow more stray light than the AERONET Cimels; however, during dust events, any reduction in $\tau_{500\mathrm{nm}}$ is estimated to be less than 0.02 [*Kinne et al.*, 1997]. The accuracy of Microtops instruments is ±0.02 for measured columnar AOD at the nominal aerosol wavelengths [*Smirnov et al.*, 2009].

2.2. Study Region

[5] Anthropogenic activities within the IGP produce pollution from urban, industrial, and rural combustion sources nearly continuously and convection-induced winds drive desert and alluvial dust into the atmosphere over the IGP during the premonsoon [*Middleton*, 1986; *Littmann*, 1991; *Chu et al.*, 2003; *Dey et al.*, 2004; *Singh et al.*, 2004; *Prasad and Singh*, 2007a; *Remer et al.*, 2008; *Gautam et al.*, 2009]. Atmospheric brown cloud formation over northern India influences the scattering and absorption of solar radiation and initiates radiative forcing effects such as solar dimming, surface cooling, and surface evaporation [*Jacobson*, 2001; *Ramanathan et al.*, 2005; *Ramanathan and Ramana*, 2005; *Pinker et al.*, 2005; *Dey and Tripathi*, 2007; *Gautam et al.*, 2010]. Atmospheric turbidity measurements were initially conducted in the 1960s over India [*Mani et al.*, 1969], and aerosol field campaigns and monitoring networks have continued to be established in order to monitor aerosol loading and other properties. Recent field campaigns included the Indian Ocean Experiment (INDOEX) [*Ramanathan et al.*, 2001; *Lelieveld et al.*, 2001], Arabian Sea Monsoon Experiment (ARMEX-II) [*Moorthy and Babu*, 2005], Indian Space Research Organization Geosphere Biosphere Programme (ISRO-GBP) (http://www.isro.org/gbp/aerosol.apx), and Integrated Campaign for Aerosols, gases, and Radiation Budget (ICARB) [*Beegum et al.*, 2008; *Moorthy et al.*, 2008; *Satheesh et al.*, 2009]. A ground-based network using the MultiWavelength Radiometers (MWR) has been deployed in India through ISRO-GBP activities [*Moorthy et al.*, 1989; *Gogoi et al.*, 2009]. Furthermore, Microtops have been operated by ISRO-GBP and others to measure aerosol optical properties in India [*Niranjan et al.*, 2005; *Singh et al.*, 2005; *Misra et al.*, 2008; *Satheesh et al.*, 2009]. In addition to these programs, the AERONET Kanpur site has collected aerosol data since January 2001 [*Singh et al.*, 2003, 2004; *Tripathi et al.*, 2005a; *Dey et al.*, 2005; *Prasad and Singh*, 2007a, 2007b, 2009].

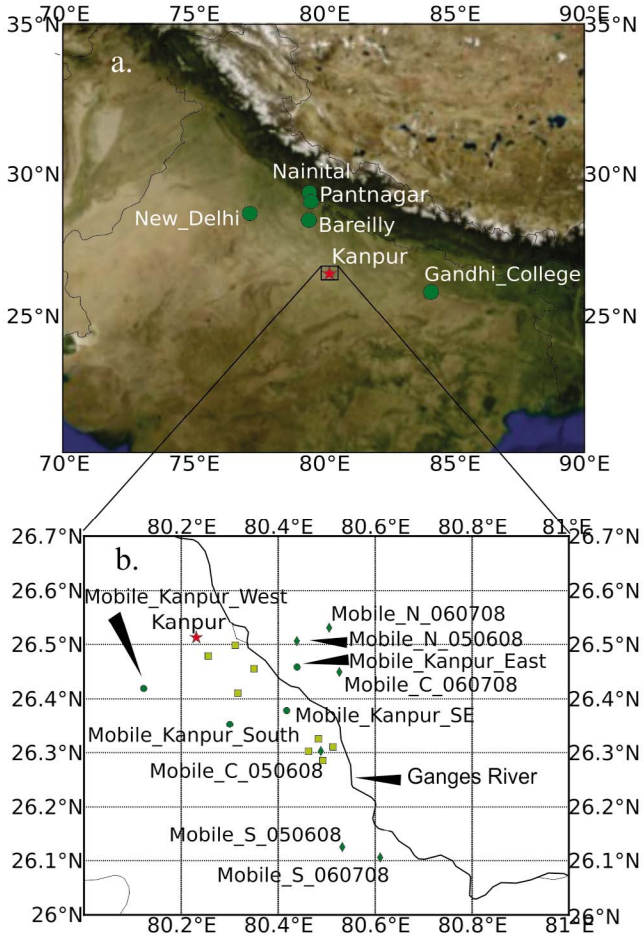

Figure 1. Atmospheric flow originating over the Thar Desert, Arabian Sea, and Bay of Bengal is restricted by the Himalayan Mountains to the north of the Indo-Gangetic Plain (IGP), allowing aerosols to accumulate here. (a) Satellite image showing the regional distribution of Cimel sites within the IGP and (b) gridded map showing the distribution of sites around Kanpur, India (26.51°N, 80.23°E). The red star represents the IIT-Kanpur site. Cimels (green symbols) and Microtops (yellow squares) were deployed at sites for Terra/Aqua (circles) and CALIPSO (diamonds) satellite overpasses. The Ganges River bisects the region.

[6] To further understand aerosol remote sensing measurements performed within the IGP, the NASA AERONET project and several international partners organized the TIGERZ multiyear, ground-based measurement campaign. TIGERZ sites were deployed spatially within the mesoscale domain based on definitions by *Orlanski* [1975]. A mesoscale-α (200–2000 km) distribution of semi-permanent AERONET sites (e.g., Bareilly and Pantnagar) was established north of Kanpur to the Himalayan foothills (Nainital) to characterize aerosols latitudinally across the IGP for the multiyear effort (Figure 1a), but these results may be presented in a later study. The TIGERZ IOP occurred in the greater Kanpur region from 1 May to 23 June 2008. Figure 1b shows the site distribution, and Table 1 provides site deployment details. Temporary sites were established within mesoscale-γ (2–20 km) and -β (20–200 km) domains using AERONET Cimels and Microtops to assess the influence of Kanpur pollution to the IGP aerosol loading as well as provide validation points for Terra, Aqua, and CALIPSO satellite retrievals [*Vaughan et al.*, 2004; *Anderson et al.*, 2005]. The low optical air mass ($m < 1.3$) during satellite overpass times precluded useful almucantar sky radiance measurements due to a limited range of measured scattering angles [*Dubovik et al.*, 2000]. A temporary deployment of sites with 15–30 km site separation, conducted from 09:45–12:45 UTC ($1.3 \leq m \leq 6.3$) on 30 May 2008, provided the first-of-its-kind spatial variability assessment of sky radiance derived AERONET aerosol properties in India.

2.3. Techniques

[7] The dominant aerosol particle size was estimated using the Ångström exponent (α), defined by the logarithms of aerosol optical depth and wavelength:

$$\alpha = -\mathrm{d}\ln[\tau(\lambda)]/\mathrm{d}\ln(\lambda) \quad (1)$$

α was calculated for the inclusive wavelength range from 440 to 870 nm using a linear fit of τ versus λ on a logarithmic scale; values closer to two indicate that small particles dominate and values approaching zero indicate larger aerosol particles dominate [*Holben et al.*, 1991; *Kaufman et al.*, 1992; *Eck et al.*, 1999; *Holben et al.*, 2001]. The spectral deconvolution algorithm (SDA) retrieved the columnar optically equivalent fine mode (τ_f) and coarse mode (τ_c) AOD as well as the fine mode fraction of AOD [$\eta = \tau_f/(\tau_f + \tau_c)$] at 500 nm. The SDA assumes a bimodal aerosol distribution, the coarse mode Ångström exponent (α_c) and its derivative (α_c') are near zero, and a second order polynomial fit of spectral AOD in logarithmic coordinates [*O'Neill et al.*, 2001, 2003]. The SDA product quality depends on the input AOD wavelengths (i.e, N $\geq$ 4 for Level 2.0), the spectral range (i.e., 380–870 nm for Level 2.0), the combination of aerosol loading and optical air mass dependence (i.e., $\tau \geq 0.02/m$), and the removal of outliers. Aerosol optical and microphysical properties were computed from inversions of sky radiance measurements simultaneously with spectral AOD at the 440, 675, 870, and 1020 nm approximate wavelengths. Almucantar-retrieved aerosol properties include the aerosol volume size distribution, complex index of refraction, phase functions, and sphericity fraction (fraction of spherical to spheroidal plus spherical particles). In addition, aerosol fine mode and coarse mode AOD, asymmetry parameter, single scattering albedo, and absorption Ångström exponent were derived from retrieved quantities [*Dubovik and King*, 2000; *Dubovik et al.*, 2002, 2006]. The AERONET Version 2 almucantar inversion algorithms, data processing, quality controls, and input surface reflectances were discussed by *Holben et al.* [2006] and *Eck et al.* [2008].

3. Aerosol Variability During the Premonsoon

[8] The AERONET long-term monitoring site at IIT-Kanpur was positioned ~17 km northwest of Kanpur's main industrial region (Figure 1). Previous work has shown that distinct seasonal patterns of aerosol properties are controlled by the monsoon (~June–September) and post-monsoon

Table 1. Instrument Inventory and Availability During the 2008 TIGERZ IOP

Location	Coordinates	Instrument	Period
Kanpur (or IIT-Kanpur)	26°30′46″N, 80°13′53″E	Cimel	1 May–23 June
Mobile_N_050608	26°30′22″N, 80°26′21″E	Cimel	6 May
Mobile_C_050608	26°18′10″N, 80°29′19″E	Cimel	6 May
Mobile_S_050608	26°07′30″N, 80°31′58″E	Cimel	6 May
Hand_N_050608	26°19′31″N, 80°29′01″E	Microtops	6 May
Hand_S_050608	26°17′08″N, 80°29′34″E	Microtops	6 May
Hand_E_050608	26°18′38″N, 80°30′49″E	Microtops	6 May
Hand_W_050608	26°18′09″N, 80°27′47″E	Microtops	6 May
Mobile_Kanpur_West (W2)	26°25′09″N, 80°07′24″E	Cimel	10, 26, and 30 May
Mobile_Kanpur_East	26°27′31″N, 80°26′22″E	Cimel	10, 26, and 30 May
Hand_Kanpur_North	26°29′55″N, 80°18′44″E	Microtops	10 and 26 May
Hand_Kanpur_South	26°24′39″N, 80°19′02″E	Microtops	10 and 26 May
Hand_Kanpur_Panki	26°28′44″N, 80°15′23″E	Microtops	10 and 26 May
Hand_Kanpur_RR	26°27′20″N, 80°21′02″E	Microtops	10 and 26 May
Mobile_Kanpur_South	26°21′10″N, 80°18′03″E	Cimel	30 May
Mobile_Kanpur_SE	26°22′43″N, 80°25′05″E	Cimel	30 May
Mobile_N_060708	26°31′50″N, 80°30′21″E	Cimel	7 June
Mobile_C_060708	26°26′58″N, 80°31′36″E	Cimel	7 June
Mobile_S_060708	26°06′21″N, 80°36′39″E	Cimel	7 June

(October–December) over Kanpur [*Singh et al.*, 2004; *Jethva et al.*, 2005; *Dey et al.*, 2005; *Eck et al.*, 2010]. Figure 2 shows the AERONET Kanpur climatology (2001–2009) of AOD (τ_{500nm}, τ_{f500nm}, τ_{c500nm}), η_{500nm}, and CWV with total AOD and CWV variability resembling seasonal fluctuations shown by *Singh et al.* [2004], *Jethva et al.* [2005], and *Eck et al.* [2010]. During the premonsoon (April–June), τ_{c500nm} increased by 0.21, while τ_{f500nm} increased by 0.03 and η_{500nm} decreased by 0.03 indicating dust contributed strongly to the τ_{500nm} increase of 0.24. A climatologically averaged CWV increase of ~3 cm between April and July over Kanpur corresponded to CWV increases observed by MWR, MODIS, and Global Positioning System (GPS) retrievals in northern India indicating the transition to the monsoon [*Moorthy et al.*, 2007; *Kumar et al.*, 2011]. Figure 3 depicts 3-day back trajectory analyses starting from Kanpur at 1000 m, derived from the NOAA Air Resources Laboratory (ARL) Hybrid Single Particle Lagrangian Integrated Trajectory (HYSPLIT) model [*Draxler and Rolph*, 2010; *Rolph*, 2010]. The April 2008 trajectories show potential aerosol transport pathways originating to the west and northwest of Kanpur in Pakistan and northern India, and May 2008 trajectories show a transition to air parcels originating in the Arabian Sea and traveling across the Thar Desert; these trajectories resemble dust transport pathways to Kanpur as shown by *Chinnam et al.* [2006] and *Prasad and Singh* [2007a]. The June 2008 and July 2008 trajectories show that most air parcels originate over the Arabian Sea and Bay of Bengal transporting moisture inland as the monsoon develops. The premonsoon (April–June) climatologically averaged τ_{c500nm} and τ_{f500nm} of 0.46 ± 0.11 and 0.22 ± 0.03, respectively, represents the dominance of long-range desert dust transport and regionally generated alluvial dust over pollution particles. Emission sources near Kanpur include vehicles powered by a variety of fuels, coal-fired power generation, leather factories, brick kilns [*Singh et al.*, 2004; *Jethva et al.*, 2005; *Dey et al.*, 2005; *Chinnam et al.*, 2006; *Prasad et al.*, 2006; *Gautam et al.*, 2009; *Eck et al.*, 2010; *Singh*, 2010], and wood fuel and agricultural waste from biomass fuel burning [*Dickerson et al.*, 2002; *Gustafsson et al.*, 2009; *Ram et al.*, 2010a, 2010b]. The interaction of fine and coarse mode particles during the premonsoon over Kanpur provided a unique opportunity to study remotely sensed properties of complex aerosol mixtures from the surface and space.

4. TIGERZ IOP Results

4.1. In-Field Instrument Comparison

[9] The AERONET reference Cimels obtain calibration at the Mauna Loa Observatory in Hawaii [*Shaw*, 1980, 1983; *Eck et al.*, 2005] and routinely cycle through the NASA Goddard Space Flight Center (GSFC) calibration facility to provide calibration transfer to Cimel and Microtops field instruments during clear and stable atmospheric conditions [*Holben et al.*, 1998; *Smirnov et al.*, 2009]. The accuracy of AERONET reference Cimels for measured columnar AOD is ~0.004 in the visible and near-infrared wavelengths and ~0.01 in the ultraviolet wavelengths [*Eck et al.*, 1999]. Although none of the AERONET reference Cimels was deployed during TIGERZ, a consistency check among the field Cimels and Microtops was performed by comparing the AOD measured at IIT-Kanpur for a 30-min period from 05:19 UTC to 05:49 UTC on 25 May 2008 (Figure 4). The AERONET Cimel #83 (or C83) was chosen arbitrarily as a "reference" to compare with other Cimels and Microtops. The C83 instrument average τ_{500nm} for the period was 0.390 ± 0.029 and the other Cimel and Microtops averages were within ±0.01 and ±0.02, respectively. The τ_{f500nm} and τ_{c500nm} averages of 0.235 ± 0.02 and 0.150 ± 0.01, respectively, from C83 indicate the presence of fine mode pollution (e.g., primarily OC, sulfates, nitrates, and BC) and dust particles. Given that Microtops and Cimels averaged AOD were similar, the apparent effect of dust particles to scatter more light into the Microtops larger field of view was not evident in this case. Overall, the Cimel and Microtops comparison showed that AOD differences were consistent with the stated field instrument uncertainties.

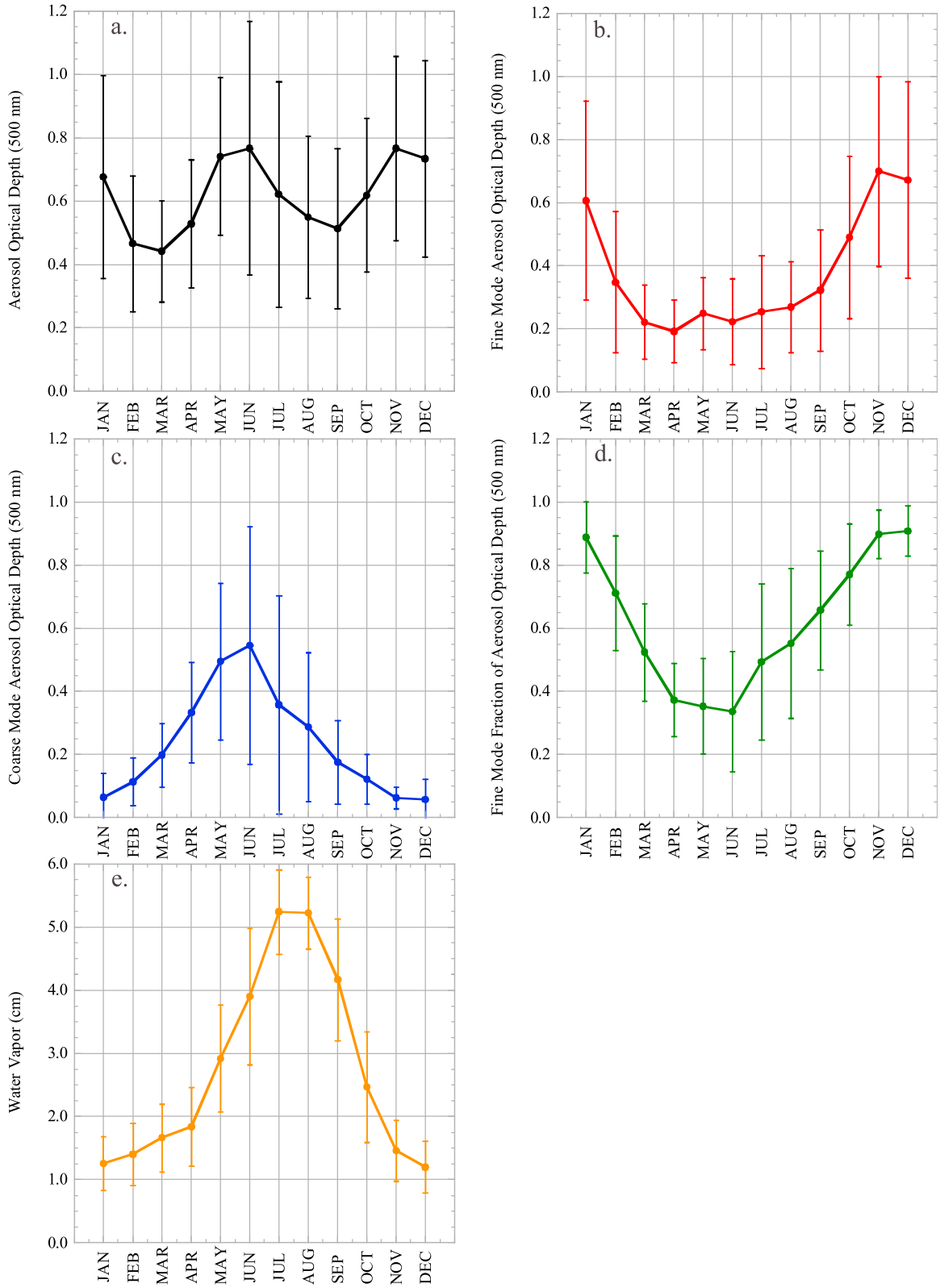

Figure 2. The 2001–2009 Kanpur multiyear monthly averages are plotted for (a) aerosol optical depth, (e) water vapor, and (b–d) spectral deconvolution algorithm (SDA) retrievals at the Level 2.0 quality level. Maximums in total and coarse mode aerosol optical depth in May and June indicate the presence of transported desert dust, and the maximum in water vapor (cm) during July and August indicates the peak of the monsoon.

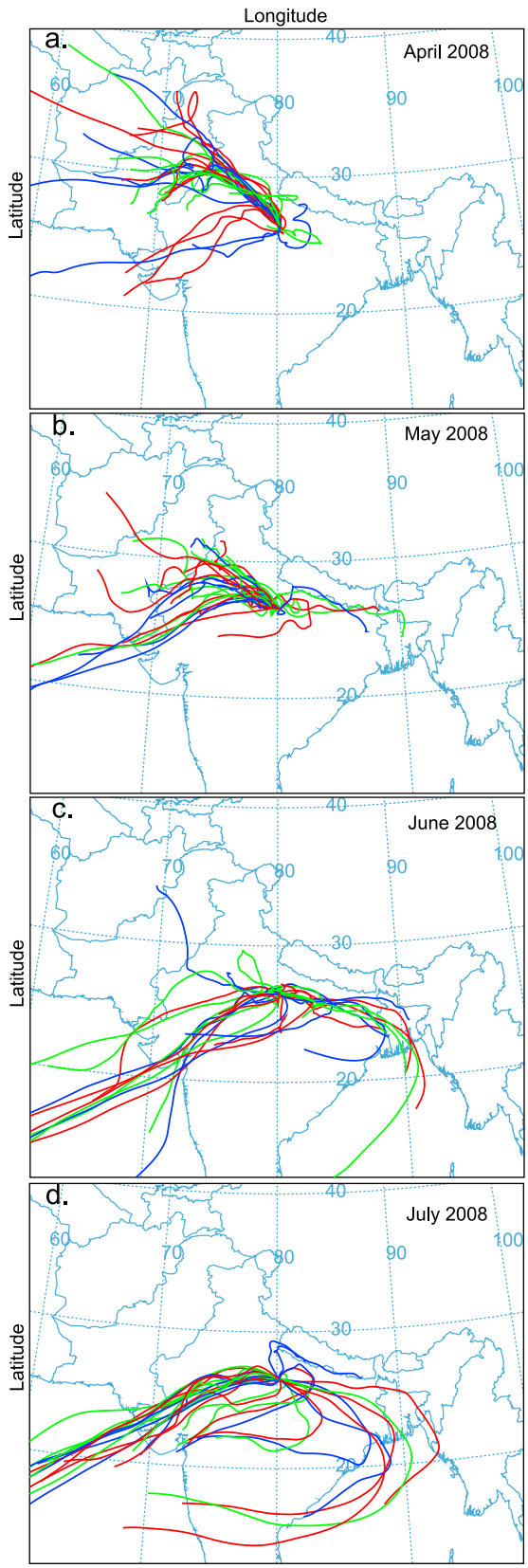

Figure 3. The NOAA HYSPLIT 3-day back trajectory analyses are shown for Kanpur, India (26.51°N, 80.23°E). The trajectories for (a–d) April–July 2008 start at 06:00 UTC and at a height of 1000 m daily. Colored trajectory lines show differentiation among trajectory days. The trajectories are based on the Global Data Assimilation System (GDAS) data available from NOAA Air Resources Laboratory at http://ready.arl.noaa.gov/HYSPLIT.php.

4.2. Spatial and Temporal Variability of Aerosol Properties

4.2.1. Spatial and Temporal Variability of Aerosol Optical Depth

[10] The TIGERZ IOP aerosol temporal variability was evaluated at IIT-Kanpur and spatial variability was determined over an area covering ~50 km^2 around Kanpur (Figure 1). Spatial variability can be analyzed by comparing one site to many nearby sites using time coincident measurements and observing the change in correlation or coefficient of variability as a function of site separation distance [*Hay and Suckling*, 1979; *Holben et al.*, 1991]. Although the TIGERZ IOP data set did not meet temporal requirements for computation of the coefficient of variability, the correlations of coincident observations at 5- and 15-min discrete intervals were analyzed for 6 and 30 May 2008; however, matchups were still statistically insignificant. Instead, TIGERZ IOP data are presented temporally as site averages and deviations and spatially as area-averages and area standard deviations derived from all sites during coincident periods.

[11] The IIT-Kanpur AERONET Cimel Level 2.0 daily averaged AOD temporal variability is shown in Figure 5. From 1 May to 12 June 2008, averaged τ_{500nm}, τ_{f500nm}, τ_{c500nm}, and η_{500nm} were 0.65 ± 0.18, 0.24 ± 0.13, 0.42 ± 0.15, and 0.36 ± 0.14, respectively, indicating high aerosol loading and mainly coarse mode particle contributions to the AOD. On temporary deployment days, IIT-Kanpur daily averages for τ_{500nm} and η_{500nm} varied from 0.28 to 0.78 and 0.21–0.37, respectively, due to transported dust. The coefficient of variation (CV) is calculated by dividing the standard deviation by the mean and multiplying by 100 to calculate the relative variability with respect to the mean. For the period, total and coarse mode aerosol loading CV was ~25–55% of the mean, which may represent dust transport and the removal of aerosols due to dry deposition and rainfall.

[12] Spatial aerosol variability was assessed using area averages for deployment days (Table 2). Most area averages for τ_{500nm}, τ_{f500nm}, and τ_{c500nm} lie within one standard deviation of the multiyear monthly averages (Figure 2); however, on 30 May 2008, area-averaged AOD (τ_{500nm} = 0.30; $\tau_{f\,500nm}$ = 0.09; τ_{c500nm} = 0.21) were anomalously low for May and June. For temporary deployments on 10 and 26 May 2008, when Microtops were located within the industrial sector and Cimels in the outer sections of Kanpur, Microtops τ_{500nm} area averages were 0.03 and 0.09 higher than Cimel area averages, respectively. Coincident period τ_{500nm} area-averaged standard deviations were up to ±0.04, indicating significant spatial variability in the measurements over different deployment configurations, whereas Microtops deviations on 6 May were only ±0.01 due to their

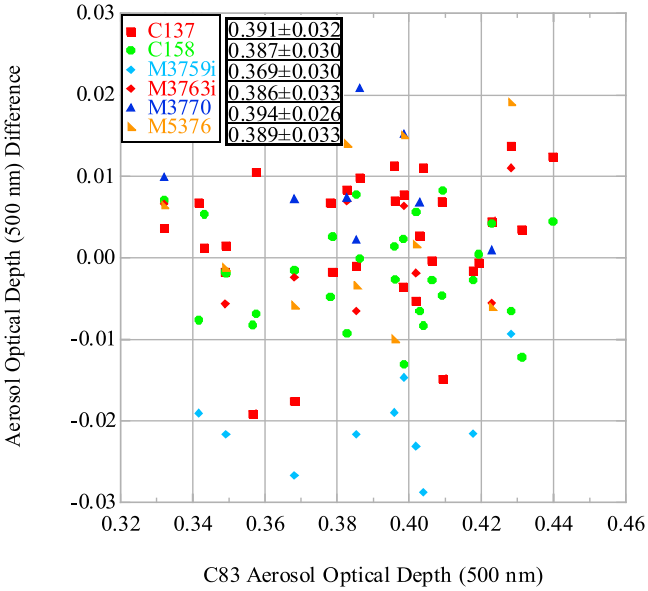

Figure 4. Cimel and Microtops aerosol optical depth at 500 nm (τ_{500nm}) measurements were compared to an arbitrary Cimel #83 (C83) at IIT-Kanpur between 05:19 UTC and 05:49 UTC on 25 May 2008 and ranged within the stated uncertainty. "C" indicates a Cimel instrument number and "M" indicates a Microtops number. An "i" at the end of a Microtops number indicates that the data were interpolated to 500 nm. The values adjacent to the legend represent the τ_{500nm} average values for each instrument during the comparison period.

proximity to each other. The Ångström exponent (α = 0.20 to 0.39) and fine mode fraction of AOD (η_{500nm} = 0.21 to 0.33) area-averages represent the presence of mainly supermicron radius or coarse mode particles region-wide on deployment days, except on 7 June 2008, when α ~0.95 and η_{500nm} of 0.55 were observed indicating a reduction of coarse mode particle AOD. Near-surface winds from the Navy Operational Global Atmospheric Prediction System (NOGAPS) model were analyzed to identify the change in aerosol loading between upwind and downwind sites. Although aerosol sources in Kanpur emit both particles (e.g., OC and BC) and precursor gases (i.e., SO_2, NO_x, etc.) into the atmosphere over the IGP [*Tripathi et al.*, 2005b; *Arola et al.*, 2011], sites downwind of the Kanpur urban center reported an increase in τ_{500nm} only up to ~0.10 near these sources. On the 30 May deployment day with only Cimels, the IIT-Kanpur and Mobile_West sites upwind of Kanpur industrial sector had lower average AOD (τ_{500nm} = 0.28 ± 0.02, 0.29 ± 0.01, respectively) than the Mobile_Southeast site (τ_{500nm} = 0.33 ± 0.02) by as much as 0.05. These upwind/downwind AOD increases were consistent with differences between Microtops within and Cimels outside the city of Kanpur on the 10 and 26 May 2008. Approximately 10–20% of the aerosol loading detected by ground-based Sun photometers on temporary deployment

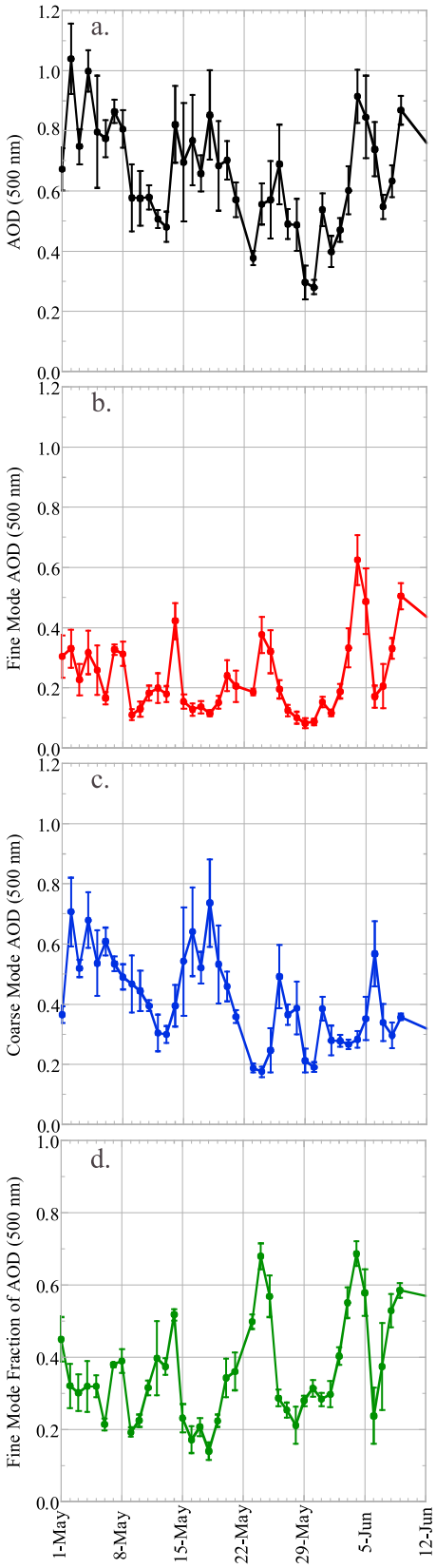

Figure 5. Substantial day-to-day variation of aerosol loading occurred during the TIGERZ IOP, possibly due to dust transport, dry deposition, and precipitation. Aerosol optical depth (AOD) daily averages of AERONET Level 2.0 are plotted for IIT-Kanpur, India, from 1 May to 12 June 2008. Temporary sites were deployed on 6 May, 10 May, 26 May, 30 May, and 7 June 2008.

Table 2. Mesoscale Deployment Day Area Averages of Aerosol Properties for Coincident Measurement Periods[a]

Group	τ	α	τ_f	τ_c	η	Time (UTC)
			6 May 2008			
All	0.75 ± 0.03	0.22 ± 0.03	0.17 ± 0.02	0.58 ± 0.03	0.23 ± 0.03	07:30–08:37
Cimel	0.77 ± 0.02	0.20 ± 0.03	0.16 ± 0.02	0.61 ± 0.01	0.21 ± 0.02	03:00–11:17
Microtops	0.73 ± 0.01	0.22 ± 0.01	0.17 ± 0.02	0.55 ± 0.03	0.24 ± 0.03	07:30–08:37
			10 May 2008			
All	0.69 ± 0.03	0.30 ± 0.06	0.19 ± 0.03	0.51 ± 0.04	0.27 ± 0.04	05:00–06:06
Cimel	0.68 ± 0.04	0.26 ± 0.06	0.16 ± 0.02	0.51 ± 0.04	0.24 ± 0.03	04:51–06:06
Microtops	0.71 ± 0.04	0.32 ± 0.05	0.21 ± 0.03	0.51 ± 0.04	0.29 ± 0.03	05:00–08:36
			26 May 2008			
All	0.88 ± 0.04	0.38 ± 0.05	0.27 ± 0.04	0.61 ± 0.03	0.31 ± 0.03	05:00–07:30
Cimel	0.84 ± 0.03	0.36 ± 0.06	0.25 ± 0.03	0.59 ± 0.02	0.30 ± 0.03	05:00–07:30
Microtops	0.93 ± 0.04	0.39 ± 0.05	0.32 ± 0.05	0.64 ± 0.03	0.33 ± 0.03	04:30–08:47
			30 May 2008			
Cimel	0.30 ± 0.02	0.38 ± 0.01	0.09 ± 0.01	0.21 ± 0.01	0.30 ± 0.01	10:05–12:30
			7 June 2008			
Cimel	0.60 ± 0.04	0.94 ± 0.03	0.33 ± 0.03	0.26 ± 0.02	0.55 ± 0.02	03:38–05:48

[a]Aerosol properties at 500 nm, except α was calculated between 440 and 870 nm.

days resulted from the Kanpur city emission contributions to the upwind aerosols comprised of a mixture of pollution and dust.

4.2.2. Spatial Variability of Aerosol Size and Absorption Properties

[13] Temporary site deployments within mesoscale-γ and -β (15–30 km site separation) domains provided a unique opportunity to acquire up to eight almucantar inversions on 30 May 2008. All of the products were processed utilizing the AERONET Level 2.0 inversion criteria [*Holben et al.*, 2006], except the input AOD may have been Level 1.5 as discussed in Section 2.1. To help interpret absorption results when τ_{440nm} was $\leq$ 0.40, a development version of the inversion code provided uncertainty estimates for each SSA retrieval. Area-averaged aerosol properties for the size distribution, single scattering albedo, and parameterizations describing the size distribution were calculated for the region covered by the temporary deployment on 30 May (09:40–12:27 UTC). The volume size distribution shows coarse mode dominated aerosol loading for all sites (Figure 6a). Calculated from volume concentration (C_v), effective radius (R_{eff}), volume mean radius (R_v), and standard deviation (σ) derived size distribution quantities in Table 3, the coefficient of variation was less than 10% of the area-averages indicating mainly uniformly sized particles over the region. Spectral SSA area-averages in Figure 6b were 0.87 ± 0.01, 0.91 ± 0.01, 0.92 ± 0.01, and 0.93 ± 0.01 for 440, 675, 870, and 1020 nm nominal wavelengths indicating spatially homogeneous absorption by aerosol particles. While average τ_{440nm} was ~0.33, the average uncertainties for SSA (Figure 6b) were approximately ±0.04 over the 440 nm to 1020 nm range, consistent with increased uncertainty during low aerosol loading ($\tau_{440nm} \leq 0.4$). The SSA uncertainty has not been quantified for the AERONET Version 2 almucantar retrievals; however, it has been estimated as ±0.03 for $\tau_{440nm} > 0.40$ for Version 1 retrievals [*Dubovik et al.*, 2002]. Although temporal SSA averages vary within the calculated uncertainty of ±0.04, Figure 6b suggests a higher probability of more absorbing aerosols downwind of Kanpur at the Mobile_SE site (where higher AOD was also found) with higher SSA values at sites north and east of the city. Black carbon particles emitted from the Panki power plant and other sources possibly increased aerosol absorption downwind of Kanpur [*Tripathi et al.*, 2005b]. Stronger spectral absorption at 440 nm represented the absorption by iron oxides in dust, whereas increasing absorption at longer wavelengths possibly represented a greater contribution of BC to the optical mixture.

4.3. Aerosol Characterization Inferred by Absorption Properties

[14] Single scattering albedo retrievals from AERONET have been compared to surface-based and airborne in situ measurements in atmospheric environments affected by biomass burning emissions, dust, or mixtures of them. *Leahy et al.* [2007], *Johnson et al.* [2009], *Müller et al.* [2010], and *Toledano et al.* [2011] show that spectral SSA differences between AERONET and in situ retrievals were well within uncertainty estimates. However, ground-based in situ measurements may exhibit large diurnal variability in SSA due to anthropogenic processes and boundary layer meteorology [*Garland et al.*, 2008]. The spectral SSA [$\omega_o(\lambda)$] and extinction AOD [$\tau_{ext}(\lambda)$] relate to the absorption AOD [$\tau_{abs}(\lambda)$] as given in equation (2). Analogous to the extinction Ångström exponent (α_{ext}) in equation (1), the absorption Ångström exponent (α_{abs}) is derived using equation (3).

$$\tau_{abs}(\lambda) = [1 - \omega_o(\lambda)] * \tau_{ext}(\lambda) \quad (2)$$

$$\alpha_{abs} = -d\ln[\tau_{abs}(\lambda)]/d\ln(\lambda) \quad (3)$$

α_{abs} was calculated for the inclusive wavelength range from 440 to 870 nm. The linear fit of τ_{abs} versus λ on a logarithmic scale cannot differentiate among particle types alone. Comparing α_{abs} to an aerosol size proxy (e.g., α_{ext} or η_{675nm}, the fine mode fraction of AOD at 675 nm from the almucantar retrieval) relates particle absorption spectral

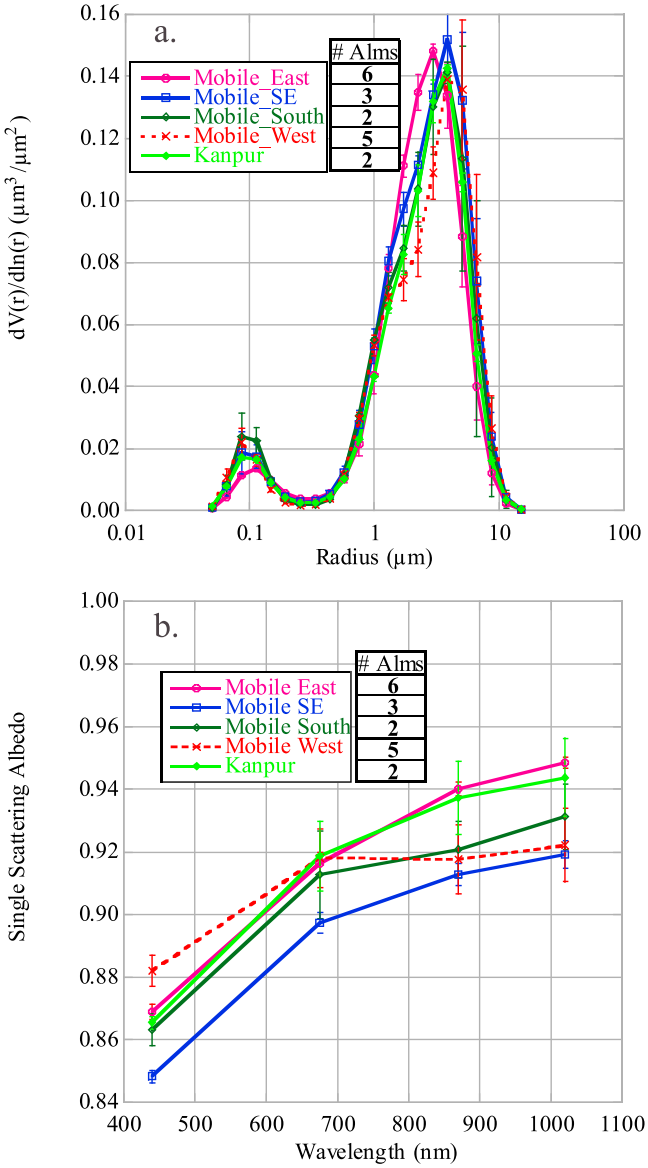

Figure 6. Data from TIGERZ IOP sites indicated spatially homogeneous, uniformly sized, spectrally absorbing pollution and dust particles. Temporally averaged almucantar retrieval plots for (a) aerosol volume size distribution and (b) spectral single scattering albedo (SSA) for the Mobile_East (pink), Mobile_Southeast (blue), Mobile_South (dark green), Mobile_West (red), and Kanpur (light green) sites are shown for the temporary site deployment on 30 May 2008. The vertical bars indicate the standard deviation in each plot. The average τ_{440nm} was 0.33 with solar zenith angle greater than 50 degrees.

dependence to particle size and potentially characterizes the dominant absorbing particle type or optical mixture. Assuming a spectrally constant refractive index, *Bergstrom et al.* [2002] suggested that small BC particles ($r < 0.01\mu$m) will have a λ^{-1} dependence or α_{abs} of 1.0, whereas larger, optically effective BC particles ($r > 0.01\mu$m) will have α_{abs} of 1.3. Deviations from these α_{abs} values occur when spectral changes in the imaginary part of the refractive index vary due to the composition of the aerosol particle [*Kirchstetter et al.*, 2004]. From Nuclepore filter measurements collected 50 km east-southeast of Beijing, China, *Chaudhry et al.* [2007] found that coarse mode particles with diameters ranging between 2.5 μm and 10 μm had a subtle increase in absorption from 350 nm to 600 nm. *Bergstrom et al.* [2007] showed that aerosol particles from different regions have distinct α_{abs} values (e.g., α_{abs} = ~2.3 for Saharan dust and Asian dust/pollution mixtures, α_{abs} = ~1.5 for South Africa biomass burning, and ~1.1 for urban/industrial,). *Lewis et al.* [2008] also showed that α_{abs} for biomass burning particles varies by fuel type, combustion phase, and organic to black carbon ratio. *Russell et al.* [2010] used AERONET Version 1 almucantar retrieval data from *Dubovik et al.* [2002] to show dust separated from other discrete aerosol types using the α_{abs} versus α_{ext} (hereafter defined as "$\alpha_{abs}/\alpha_{ext}$") relationship to classify data clusters (e.g., α_{abs} = ~1.2 to ~3.0 for dust, α_{abs} = ~1.2 to ~1.5 for biomass burning, and α_{abs} = ~0.75 to ~1.3 for urban/industrial), although particles with absorption dominated by BC content (i.e., urban and biomass burning aerosols) were less defined and required more information [*Giles et al.*, 2010].

[15] Both the $\alpha_{abs}/\alpha_{ext}$ and α_{abs} versus η_{675nm} (hereafter defined as "$\alpha_{abs}/\eta_{675nm}$") relationships were examined with AERONET Version 2, Level 2.0 AOD and almucantar retrievals for Kanpur. For all months from 2002 to 2008, the $\alpha_{abs}/\alpha_{ext}$ and $\alpha_{abs}/\eta_{675nm}$ relationships (Figures 7a and 7c) show a nonlinear dependence over the aerosol size ranges, whereas the sphericity fraction, generally valid for only $\alpha_{ext} < 1.0$ according to *Dubovik et al.* [2006], has a strong transition from non-spherical to spherical particles around α_{ext} of ~1.3 or η_{675nm} of ~0.66. The "Mostly Dust" category [i.e., $\alpha_{ext} \leq 0.5$ ($\eta_{675nm} \leq 0.33$) and sphericity fraction < 0.2] with $\alpha_{abs} > 2.0$ and the "Mostly BC" category [i.e., $\alpha_{ext} > 0.8$ ($\eta_{675nm} > 0.66$) and sphericity fraction ≥ 0.2] with $1.0 < \alpha_{abs} \leq 2.0$ are consistent with results reported by *Bergstrom et al.* [2007] and *Russell et al.* [2010]. The "Mostly Dust" category identifies aerosol mixtures where iron oxide in dust is the dominate absorber and the "Mostly BC" category represents a mixture of biomass burning and urban/industrial emissions with BC as the dominant absorber, although other absorbers such as brown carbon and soot carbon may exist [*Gustafsson et al.*, 2009]. The $\alpha_{ext} > 0.8$ ($\eta_{675nm} > 0.66$) and $\alpha_{abs} > 2.0$ may indicate a greater organic carbon concentration [*Arola et al.*, 2011]. The $\alpha_{abs}/\alpha_{ext}$ and $\alpha_{abs}/\eta_{675nm}$ relationships during the premonsoon (Figures 7b and 7d) revealed the dominance of large particles with α_{abs} ranging mainly from 1.25 to 3.0. Centered on the maximum density at α_{ext}~0.5 (η_{675nm} ~0.33) with α_{abs}~1.5, the "Mixed BC and Dust" category likely represents an optical mixture of fine mode BC and coarse mode dust as the dominant absorbers. Notably, these classifications are complicated by the fact that 6% of the Kanpur Level 2.0 data set (2002–2008) had $\alpha_{abs} < 1.0$, where α_{abs} ~1.0 is often identified as indicative of exclusively BC absorption. *Bergstrom et al.* [2007] found that $\alpha_{abs} < 1.0$ occurred frequently in Particle Soot Absorption Photometer (PSAP) data and suggested that the imaginary refractive index may decrease with wavelength due to absorption AOD spectral dependence or the low α_{abs} values are related to measurement uncertainties. For AERONET data, $\alpha_{abs} < 1.0$ may be related to higher SSA retrieval uncertainty for low aerosol loading cases

Table 3. Area-Averaged Aerosol Volume Size Distribution Quantities for Fine Mode (*f*) and Coarse Mode (*c*) Aerosols on 30 May 2008[a]

Site	R_{eff} (μm)		V_c		R_v (μm)		σ		N
	f	*c*	*f*	*c*	*f*	*c*	*f*	*c*	
Mobile_Kanpur_East	0.12	2.11	0.016	0.227	0.14	2.52	0.52	0.59	6
Mobile_Kanpur_SE	0.11	2.20	0.019	0.246	0.12	2.73	0.50	0.64	3
Mobile_Kanpur_South	0.10	2.17	0.021	0.235	0.11	2.67	0.43	0.64	2
Mobile_Kanpur_West	0.09	2.23	0.018	0.223	0.11	2.84	0.46	0.67	5
Kanpur	0.11	2.21	0.018	0.212	0.12	2.71	0.50	0.62	2
Area Average	0.11 ±0.01	2.18 ±0.05	0.018 ±0.001	0.229 ±0.013	0.12 ±0.01	2.69 ±0.12	0.48 ±0.04	0.63 ±0.03	

[a]Corresponds to Figure 6a.

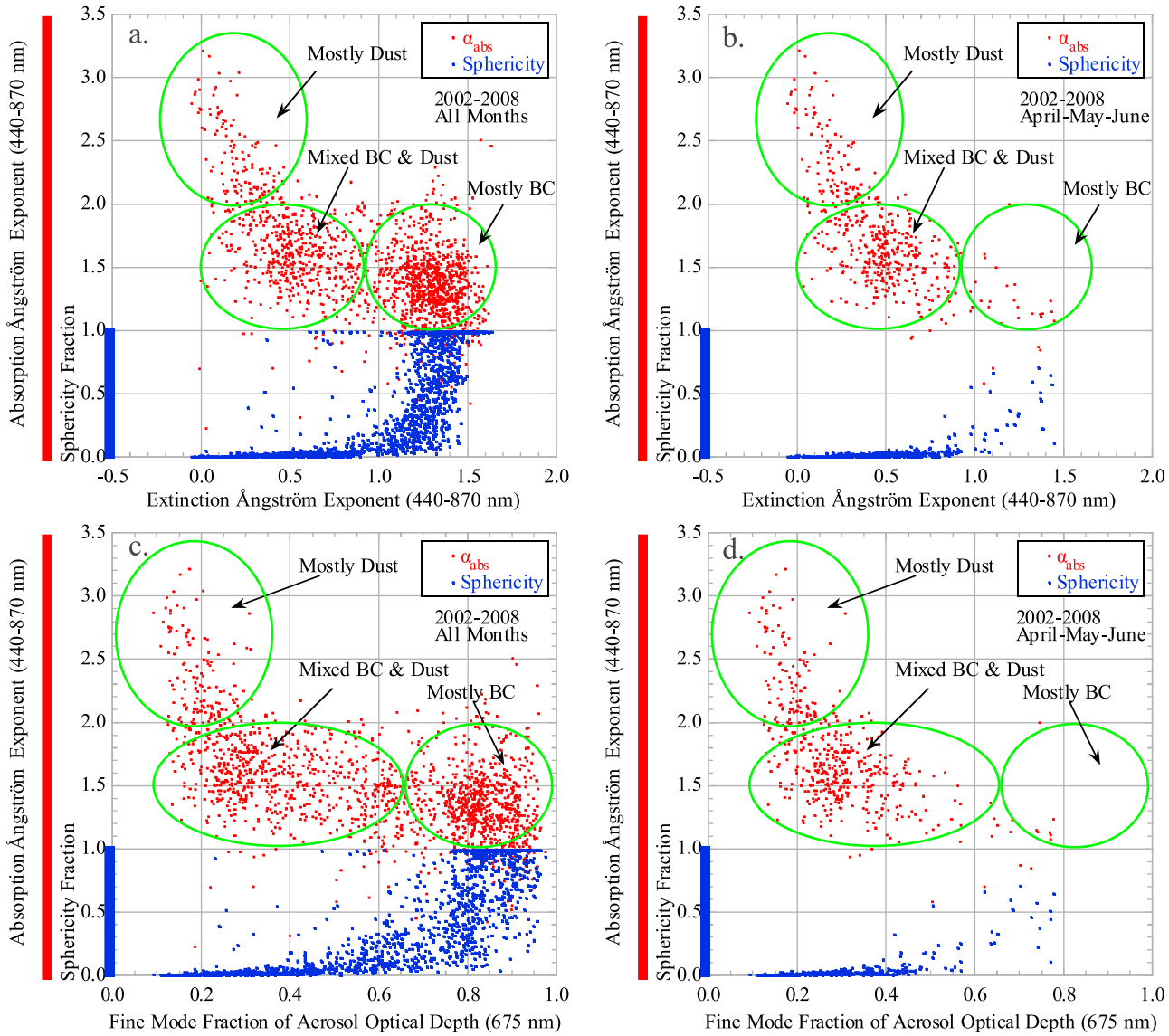

Figure 7. Level 2.0 absorption Ångström exponent (α_{abs}) and sphericity fraction as a function of extinction Ångström exponent (α_{ext}) and fine mode fraction of AOD at 675 nm (η_{675nm}; from the almucantar inversions) from the Kanpur AERONET record (2002–2008) during (a, c) all seasons and (b, d) April–May–June. α_{abs} is plotted from 0.0 to 3.5 (red) and sphericity fraction is plotted from 0.0 to 1.0 (blue). The green ellipses represent probable aerosol mixture categories. α_{abs} of 1.0 indicates λ^{-1} dependence, and a sphericity fraction of 1.0 indicates a 100% spherical particle.

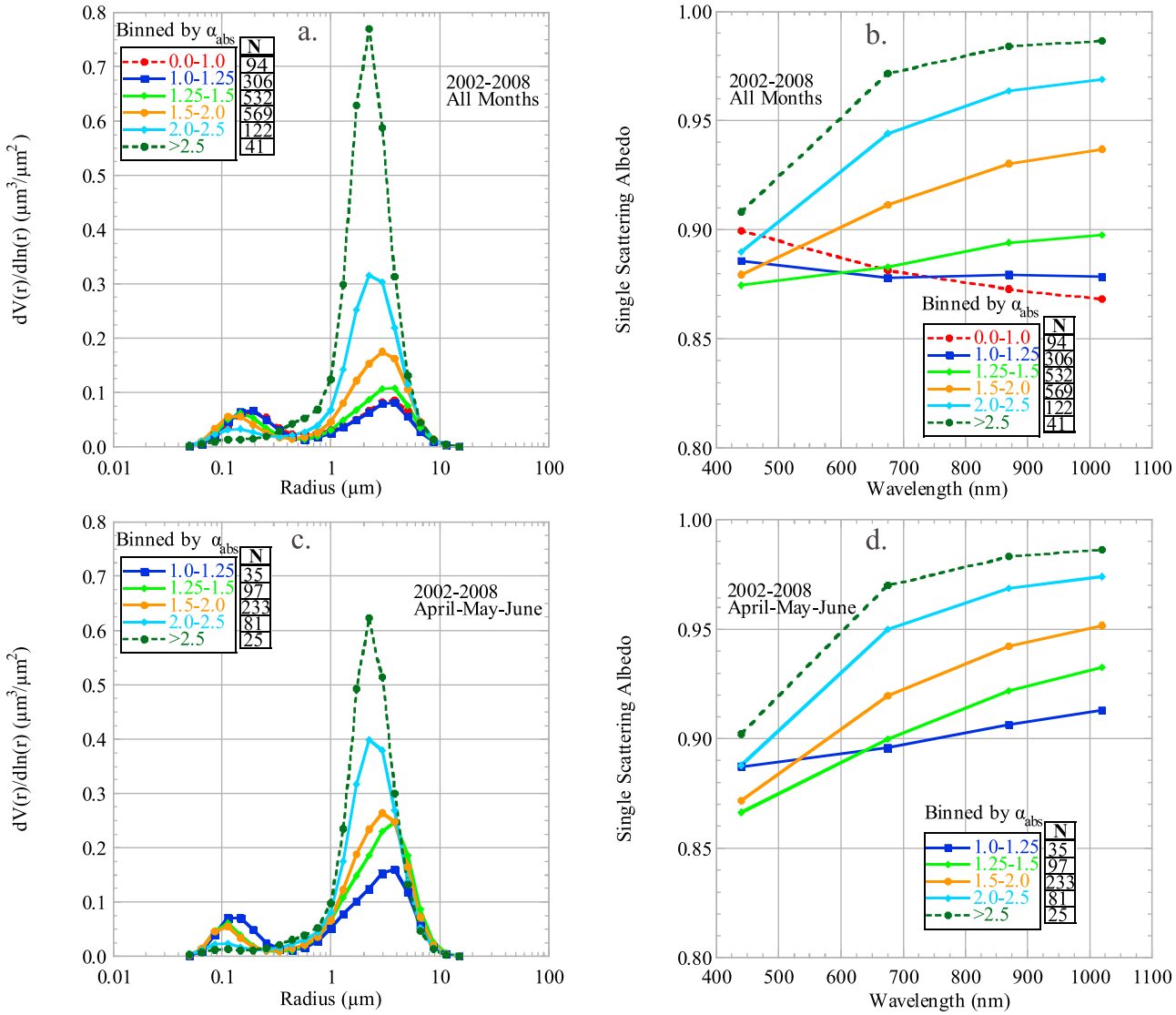

Figure 8. As absorption Ångström exponent decreased to 1.0, coarse mode particles became less dominant for both the annual cycle and premonsoon. Further, single scattering albedo transitioned from spectra representing dust (i.e., typical iron oxide absorption in the blue wavelength region and relatively weak absorption in the near-infrared) to urban/industrial pollution containing black carbon (i.e., stronger absorption in longer wavelengths). Level 2.0 almucantar retrievals from the Kanpur AERONET (2002–2008) during (a, b) all seasons and (c, d) April–May–June for aerosol volume size distribution (a, c) and for SSA (b, d) averaged by α_{abs} bins. Averages in which N < 25 were removed from the plots.

[*Dubovik et al.*, 2000; *Giles et al.*, 2010], nonlinearity of absorption optical depth [*Eck et al.*, 2010], the quality of the almucantar measurement sequence, and the spectral range chosen for the calculation. Some $\alpha_{abs} < 1.0$ cases at Kanpur revealed potential measurement inconsistencies between Sun and sky collimators (e.g., spider webs or dust) or possible diffuse cloud contamination (e.g., uniform optically thin cirrus). *Kirchstetter et al.* [2004] reported α_{abs} values below 1.0 for similar wavelength regions using in situ measurements, therefore some AERONET retrievals with $\alpha_{abs} < 1.0$ may be the result of actual spectral variation.

[16] Remotely sensed aerosol retrievals cannot determine whether BC coats dust; however, the likelihood for this interaction increases over the IGP during the premonsoon and results from *Arimoto et al.* [2006] and *Guo et al.* [2010] in China and *Dey et al.* [2008] in India suggest this interaction is likely. The volume size distribution and SSA retrievals were binned based on α_{abs} (Figure 8). As α_{abs} decreases to 1.0, coarse mode particles became less dominant for both the annual cycle and premonsoon (Figures 8a and 8c). In Figures 8b and 8d, SSA transitioned from spectra representing dust (i.e., typical iron oxide absorption in the blue wavelength region and relatively weak absorption in the near-infrared) to urban/industrial pollution containing BC (i.e., stronger absorption in longer wavelengths); the interpretation of these SSA spectra are consistent with results reported by *Dubovik et al.* [2002], *Singh et al.* [2004], *Eck et al.* [2003, 2005, 2008, 2009], *Prasad and Singh* [2007a], and *Derimian et al.* [2008]. Single scattering albedo binned by α_{abs} was further partitioned based on

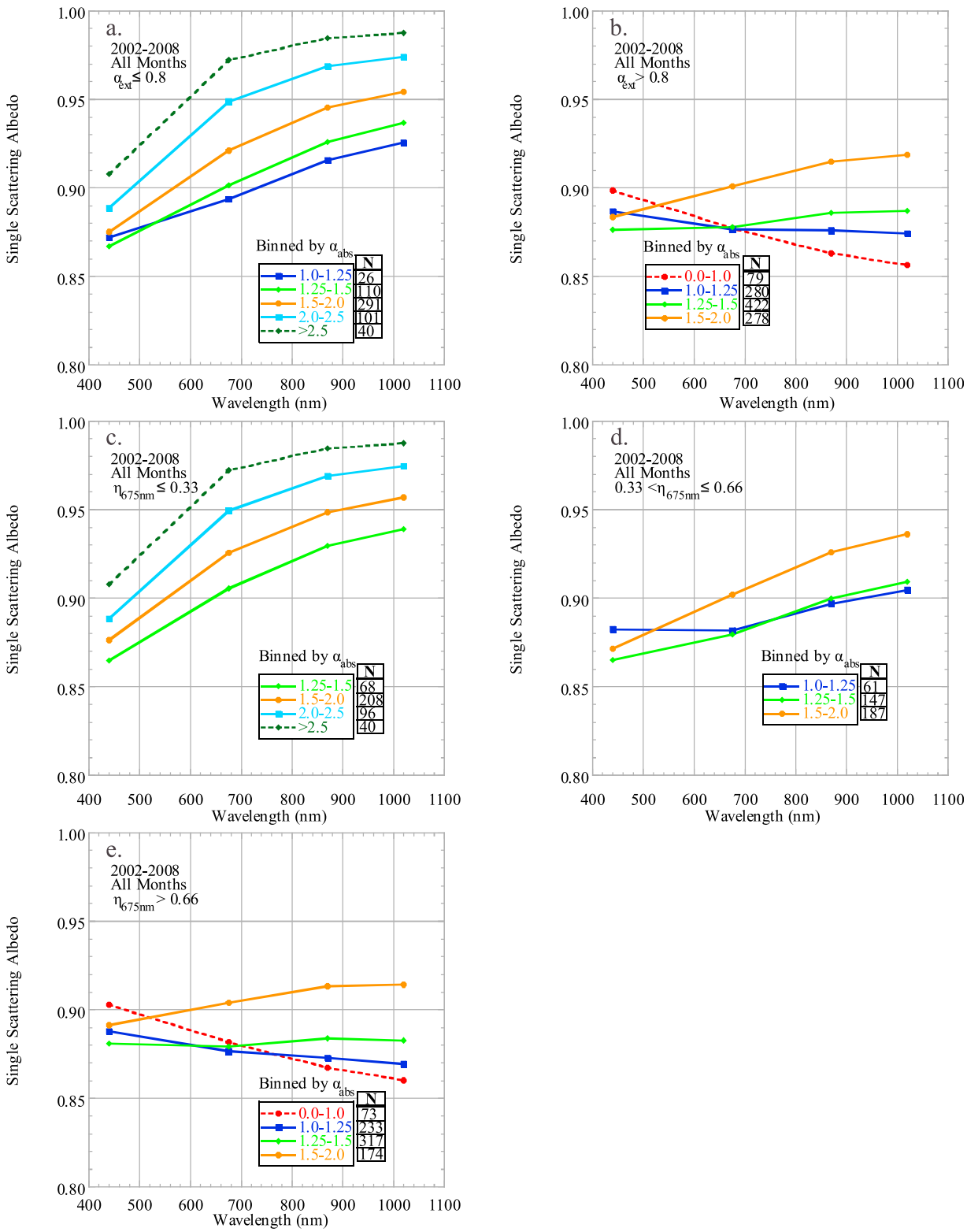

Figure 9. Level 2.0 SSA data were averaged for α_{abs} bins and further partitioned based on α_{ext} and η_{675nm} using Kanpur AERONET (2002–2008). (a) The case for large particle-dominated conditions (i.e., α_{ext} is ≤ 0.8); (b) the case for small particle-dominated conditions (i.e., $\alpha_{ext} > 0.8$); (c) mainly coarse mode particles ($\eta_{675nm} \leq 0.33$); (d) mixed size particles ($0.33 < \eta_{675nm} \leq 0.66$); and (e) mainly fine mode particles ($\eta_{675nm} > 0.66$). Averages in which N < 25 were removed from the plots.

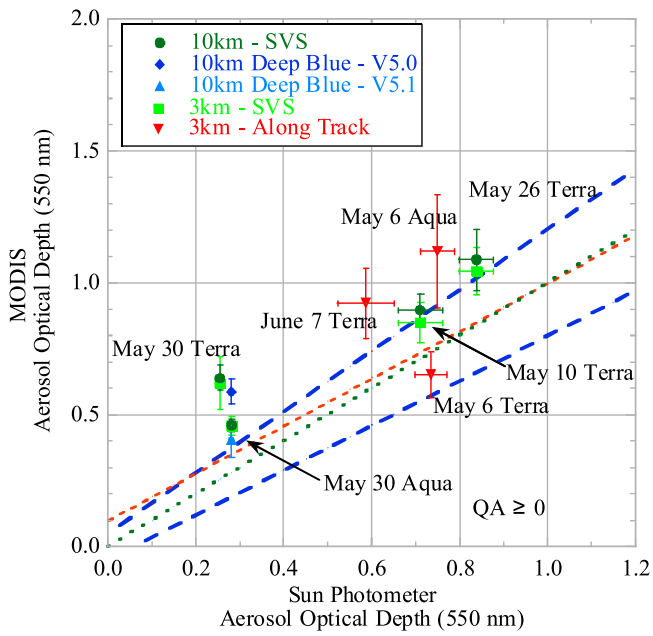

Figure 10. MODIS AOD retrievals with QA ≥ 0 were biased high with respect to TIGERZ IOP area-averaged measurements. MODIS AOD 3 km retrievals improved spatial representativeness during some conditions (e.g., cloudy skies) that prohibited the retrieval of 10 km products. Area-averaged MODIS (MOD04_L2/MYD04_L2) 3 km and 10 km τ_{550nm} versus area-averaged Sun photometer (Cimel and Microtops) τ_{550nm} were compared for each temporary deployment. The vertical and horizontal error bars indicate standard deviations for MODIS and Sun photometer area averages, respectively. The blue dashed lines indicate the calculated MODIS uncertainty compared to Sun photometer AOD. The green dotted line is the one-to-one line. The red dashed line shows the trend in reported MODIS retrievals, for all AERONET sites globally, based on a several validation studies as reported by *Levy et al.* [2007].

the α_{ext} intervals of 0.0–0.8 and 0.8–2.0 and η_{675nm} intervals of 0.0–0.33, 0.33–0.66, and 0.66–1.0 (Figure 9). Strong absorption is noted at 440 nm relative to longer wavelengths due to large dust particles, but increasing absorption at longer wavelengths indicates a greater absorption contribution by fine mode BC. For nearly 75% of cases, mainly large particles (α_{ext}~0.0–0.8) were classified as "Mostly Dust" and mainly small particles (α_{ext}~0.8–2.0) were classified as "Mostly BC" (see ellipses in Figure 7), whereas the other 25% of the cases in both size categories were classified as "Mixed BC and Dust." Approximately 33% of retrievals were classified as "Mostly Dust" and 67% as "Mixed BC and Dust" for coarse mode particles ($\eta_{675nm} \leq 0.33$), whereas, by definition, all of the retrievals were classified as "Mostly BC and Dust" for mixed size particles ($0.33 < \eta_{675nm} \leq 0.66$) and "Mostly BC" for fine mode particles ($\eta_{675nm} > 0.66$). The optical mixture of dust transported over or mixed with pollution dominates during the premonsoon, and the small particle dominated optical mixtures are consistent with pollution occurring during winter [*Singh et al.*, 2004].

4.4. Satellite Validation

[17] Terra and Aqua MODIS satellite data were evaluated using the TIGERZ IOP data set. Collection 5 (C005) and 5.1 (C051) processing utilizes the MODIS dark target and Deep Blue algorithms [*Kaufman et al.*, 1997; *Remer et al.*, 2005; *Hsu et al.*, 2006; *Levy et al.*, 2007]. Retrievals of MODIS (MOD04_L2/MYD04_L2) τ_{550nm} were compared to ground-based measurements of AOD interpolated to 550 nm using the linear fit of the logarithms of AOD and wavelength. The subset statistics generated from 10 km MODIS AOD granules were computed following the procedure presented by *Ichoku et al.* [2002] for a 50 × 50 km (5 × 5 pixels) box, whereas 3 km granules used a 48 × 48 km (16 × 16 pixels) box around the Kanpur AERONET site. The MODIS/AERONET matchups were performed when MODIS had at least five pixels for the overpass and AERONET had at least two observations within ±30 min. Modifying the procedure to use actual geographic pixel dimensions for the bounding box or decreasing the average time from overpass for ground-based measurements had a negligible effect on statistics when compared to the method suggested by *Ichoku et al.* [2002]. Each 10 km MODIS product provided quality assurance (QA) flags to indicate the confidence level of each pixel ranging from 0 (poor) to 3 (very good) and were generated based on the presence of clouds, fitting errors, limits on AOD, and semi-bright land surface in addition to other quality checks [*Remer et al.*, 2009], although these QA flags were not available for the 3 km MODIS product.

[18] The Terra and Aqua MODIS comparisons for the five TIGERZ deployment days are shown in Figure 10 for MODIS aerosol product QA flags ≥ 0. Depending on the deployment day, Sun photometer data represent Cimel and Microtops or Cimel area averages (Table 2). As indicated by *Remer et al.* [2008], MODIS retrievals with QA < 3 are generally used for qualitative rather than quantitative purposes; however, due to the lack of QA = 3 retrievals for 10 km and the 3 km products, 0 ≤ QA < 3 flags were analyzed here. In Figure 10, the overpass matchups for these five days show higher MODIS τ_{550nm} values over most of the range when compared to Sun photometers consistent with *Jethva et al.* [2006]. This finding is not consistent with other studies showing MODIS AOD biases as a function of ground-based Sun photometer AOD, where MODIS AOD is overestimated at low AOD and underestimated at high AOD [*Remer et al.*, 2008]; however, the small sample size here limits the robustness of the trend analysis. In this case, very high MODIS τ_{550nm} values are likely the result of non-spherical particle scattering by dust aerosols over the semi-bright surface reducing the contrast between the atmosphere and surface [*Jethva et al.*, 2006]. In comparison to the MODIS 10 km retrievals, the MODIS 3 km retrievals show similar or better agreement with the ground-based instruments (Figure 10). In addition, three matchups were made on 6 May 2008 (Terra and Aqua) and 7 June 2008 (Terra). For the Terra overpass on 7 June 2008, clouds were visible in the northern portion of the 50x50 km domain when 10 km MODIS retrievals were not available; however, the immediate vicinity of Kanpur did not have clouds and allowed the retrieval of 3 km MODIS AOD pixels. Consistent with results from *Johnson et al.* [2009] and *Ginoux et al.* [2010],

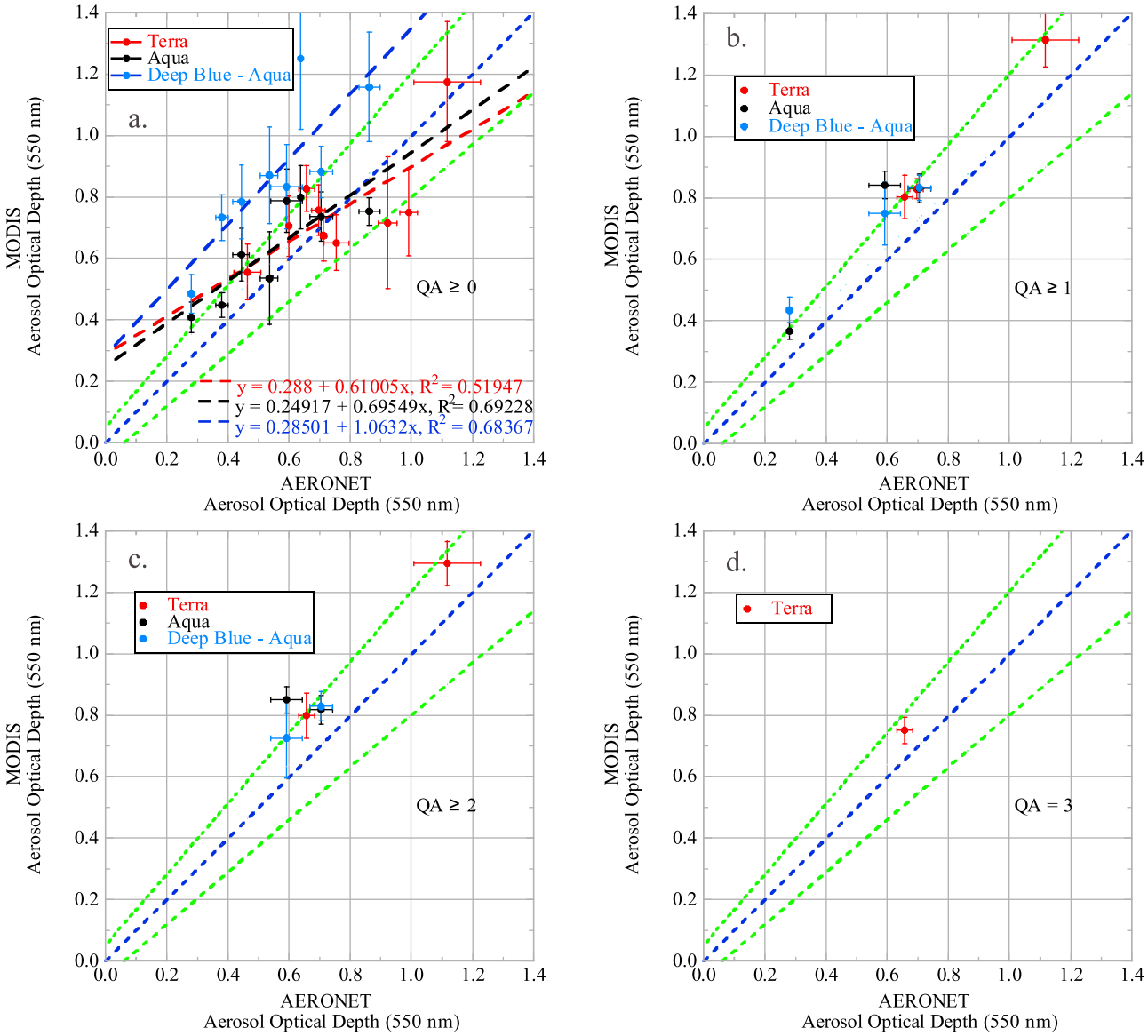

Figure 11. MODIS AOD 10 km retrievals with the lowest quality assurance (QA ≥ 0) had moderate correlation with the Kanpur AERONET site, whereas retrievals with QA > 0 were limited in number over the semi-bright land surface. Area-averaged MODIS (MOD04_L2/MYD04_L2) 10 km τ_{550nm} versus Kanpur AERONET τ_{550nm} compared from 1 May to 9 June 2008 and partitioned for each QA level (a) ≥ 0, (b) ≥ 1, (c) ≥ 2, and (d) 3 for the Terra MODIS, Aqua MODIS, and Aqua Deep Blue MODIS algorithms. The vertical and horizontal error bars indicate the standard deviations for the MODIS area average and the AERONET temporal average, respectively.

on 30 May 2008, the Aqua C051 Deep Blue retrieval shows improvement over the Aqua C005 Deep Blue retrieval with a reduction in τ_{550nm} by ~0.18 due to an improved characterization of the land surface.

[19] The MODIS 10 km τ_{550nm} was evaluated using the AERONET long-term monitoring Cimel at IIT-Kanpur during the TIGERZ IOP (1 May 2008 to 23 June 2008). Figure 11 shows moderate correlation between MODIS and AERONET with R^2 values (and root mean square error in parentheses) of 0.52 (0.12), 0.69 (0.11), and 0.68 (0.17) for Terra-MODIS, Aqua-MODIS, and Aqua-Deep Blue MODIS, respectively. These correlations with respect to other validation exercises at Kanpur were slightly lower than those reported by *Tripathi et al.* [2005a] (R^2 = 0.72) for dust events using MODIS Collection 4 (C004) Level 2 data set in 2004, higher than those reported by *Prasad and Singh* [2007b] (R^2 = 0.29) using C004 Level 3 MODIS AOD during the premonsoon season (April–June), and lower than those reported by *Jethva et al.* [2007b] (R^2 = 0.83) for MODIS C005 from 2002 to 2005. Furthermore, the MODIS and AERONET correlations are similar to those reported by *Dey and Di Girolamo* [2010] (R^2 = 0.69) for Multiangle Imaging Spectroradiometer (MISR) over Kanpur from 2001 to 2008, higher than those reported by *Kar et al.* [2010] (R^2 = 0.25) for CALIPSO over Kanpur from 2006 to 2009, and similar to those reported by *Hyer et al.* [2011]

Table 4. Potential and Actual MODIS, AERONET Level 2.0 (L2), and AERONET Level 2.0 + Level 1.0 Screened (L2 + L1) Matchups from 1 May to 23 June 2008

Matchups	Potential MODIS	Potential AERONET L2	Potential AERONET L2 + L1	Actual
Satellite	Days	Days	Days	Days
Terra	18	9	13	9
Aqua	20	16	18	8

(R^2 = 0.71) for MODIS C005 Level 2 data compared to all AERONET sites on the Indian sub-continent from 2005 to 2008. The Terra and Aqua-MODIS retrievals had better agreement with AERONET within the stated MODIS uncertainty [*Remer et al.*, 2008] than Aqua-Deep Blue retrievals. For Figure 11a, the linear regression through each standard MODIS retrieval suggests an overestimation at low τ_{550nm} and underestimation at high τ_{550nm} with the inflection point near 0.45; this result is a well-known bias in the MODIS retrieval and depends on particle size distribution, shape, and absorption [*Ichoku et al.*, 2005; *Levy et al.*, 2005; *Remer et al.*, 2005]. The linear regression for the Aqua Deep Blue retrieval gives a slope near 1.0 and high offset of ~0.29 due to issues with the assumed bidirectional reflectance distribution function (BRDF) model over the Kanpur region. Quality assurance flags 1, 2, and 3, representing increased confidence in the retrieved pixel, were evaluated and used to remove significant portions of the MODIS data. In Figures 11b–11d, higher quality retrievals show all MODIS products were biased high when compared to AERONET. For these overpasses, significant cloud cover was not identified by either on-site observers or by manual inspection of MODIS Rapid Response true color images generated for the Kanpur AERONET site. On 18 May 2008, dust over the semi-bright surface reduced the aerosol to surface contrast and resulted in no Terra/MODIS aerosol retrievals on this cloud-free day, while Level 2.0 AERONET measurements were available during the overpass time. The MISR instrument had one cloud-free scene on 18 May 2008, where MISR retrieved a τ_{558nm} of 0.70 [R. Kahn, personal communication, 2010] and the corresponding AERONET Kanpur interpolated τ_{558nm} was 0.72 for ±30 min of the Terra overpass at 05:15 UTC. However, *Dey and Di Girolamo* [2010] showed that MISR AOD typically underestimated Kanpur AERONET observations when analyzing all seasons similar to results from *Kahn et al.* [2005] and *Prasad and Singh* [2007b].

[20] Further investigation of the ground-based data revealed that some data were removed by the AERONET cloud-screening algorithm during cloud-free periods when aerosols were primarily dust. Dust occasionally exhibits a similar spectral AOD signature to spectral cloud optical depth by having almost no spectral dependence and high triplet variability causing the AERONET cloud-screening algorithm to misclassify dust as cloud [*Smirnov et al.*, 2000]. During over-cloud-screened days, Level 1.0 AOD data were inspected for anomalies, verified with observer sky condition logs, and incorporated into the MODIS overpass comparison to provide additional valid points. Potential MODIS days were based on retrievals made for QA ≥ 0 during mainly cloud-free and low aerosol loading conditions. Re-inspected AERONET data provided 29 additional validation points within ±30 min of MODIS overpass for MODIS/AERONET matchups between 1 May 2008 and 23 June 2008. Reconstituted AERONET points (within ±30 min of satellite overpass) increased observations available for four previously identified MODIS/AERONET matchups (i.e., one for Terra and three for Aqua) and added two or more AERONET validation points to enable six additional potential MODIS/AERONET matchups (i.e., four for Terra and two for Aqua). As a result, these additional AERONET validation points increased the potential MODIS/AERONET matchups by 24% from 25 to 31 (Table 4). During the period, 55 MODIS retrieval days were possible over Kanpur; however, less than 50% of the overpass days (18 days for Terra and 20 days for Aqua) were retrieved by MODIS due to clouds, elevated dust, or surface reflectance issues. In summary, both AERONET and MODIS algorithms occasionally misclassified dust as clouds, and additionally, semi-bright surface effects sometimes resulted in screening by the MODIS algorithm over the IGP during the premonsoon.

[21] The evaluation of MODIS aerosol products over the IGP has shown the need for additional algorithm or parameterization improvements. MODIS retrievals for C005 and C051 overestimated and under-sampled aerosol properties when compared to TIGERZ IOP measurements at Kanpur; this is consistent with MODIS C004 retrieval biases identified by *Jethva et al.* [2007a] over the IGP during the premonsoon. However, *Jethva et al.* [2007b, 2010] have adjusted both the absorbing aerosol model assumed by the MODIS C005 algorithm and the surface reflectance to produce more accurate retrievals. Although spatially distributed MODIS aerosol retrievals are commonly compared to ground-based Sun photometer point measurements, the TIGERZ IOP has provided a unique data set on the same spatial scale to provide a more robust validation of satellite retrievals.

5. Conclusions

[22] The international 2008 TIGERZ experiment intensive operational period was conducted in the Indo-Gangetic Plain around Kanpur, India, during the premonsoon (April–June). Mesoscale-distributed Sun photometers quantified temporal and spatial variability of aerosol properties to determine Kanpur urban emission contributions to upwind IGP aerosol loading and validate aerosol retrievals from satellites. Using the long-term Kanpur data set, the climatological aerosol variability during the premonsoon was discussed and aerosol absorption and size relationships were evaluated to determine dominant aerosol absorbing types or mixtures. The study yielded the following conclusions:

[23] (1) TIGERZ intensive operational period Sun photometers quantified AOD increases up to ~0.10 within and downwind of the city due to local Kanpur emissions including black carbon. Approximately 10–20% of the aerosol loading detected by ground-based Sun photometers on temporary deployment days resulted from the Kanpur city emission contributions to the upwind aerosols comprised of a mixture of pollution and dust.

[24] (2) For a mesoscale case study day with 15–30 km site separation, relative variability was less than 10% of the

area-averages for parameterizations describing the size distribution indicating mainly uniformly sized particles over Kanpur. Spectral single scattering albedo area-averages (0.87–0.93) had stronger absorption at 440 nm due to iron oxides in dust and indicated spatially homogeneous absorption by black carbon and dust particles.

[25] (3) Aerosol absorption (absorption Ångström exponent) and size (extinction Ångström exponent and fine mode fraction of AOD) relationships showed a nonlinear dependence over the aerosol size ranges and allowed for the determination of dominant absorbing aerosol types. These relationships along with averaged single scattering albedo spectra were used to categorize black carbon and dust as dominant absorbers and identify a third category where both black carbon and dust dominate absorption. As absorption Ångström exponent decreased to 1.0, coarse mode particles became less dominant for both the annual cycle and premonsoon. Further, single scattering albedo transitioned from spectra representing dust (i.e., typical iron oxide absorption in the blue wavelength region and relatively weak absorption in the near-infrared) to urban/industrial pollution containing black carbon (i.e., stronger absorption in longer wavelengths).

[26] (4) MODIS AOD 3 km and 10 km retrievals with the lowest quality assurance (QA $\geq$ 0) flags were biased high with respect to TIGERZ IOP measurements. MODIS AOD 3 km retrievals improved spatial representativeness during some conditions (e.g., clouds) that prohibited the retrieval of 10 km products. MODIS AOD 10 km retrievals with QA $\geq$ 0 had moderate correlation (R^2 = 0.52–0.69) with the Kanpur AERONET site, whereas retrievals with QA > 0 were limited in number over the semi-bright land surface. AERONET and MODIS algorithms occasionally misclassified dust as clouds over the IGP during the premonsoon.

[27] **Acknowledgments.** The NASA AERONET project was supported by Michael D. King, who retired in 2008 from the NASA EOS project office, and by Hal B. Maring, Radiation Sciences Program, NASA Headquarters. The authors would like thank all of the more than 30 participants and collaborators in the NASA/GSFC TIGERZ campaign effort, including many Indian researchers and graduate students as well as other national and international agencies that provided personnel and equipment to perform the study. The authors thank the AERONET team for calibrating and maintaining instrumentation and processing these data. The authors would like to recognize Harish Vishwakarma at IIT-Kanpur for field support during TIGERZ and continued support of the long-term Kanpur AERONET site. The authors gratefully acknowledge the NOAA Air Resources Laboratory (ARL) for providing data from the HYSPLIT transport and dispersion model and/or READY website (http://www.arl.noaa.gov/ready.php) used in this publication. The authors thank Jeffrey Reid and two anonymous reviewers for their constructive comments on an earlier version of the manuscript. Furthermore, the authors recognize with great sadness their deceased coauthor Wilber Wayne Newcomb for his major contributions to the TIGERZ campaign and AERONET.

References

Anderson, T. L., et al. (2005), An "A-train" strategy for quantifying direct climate forcing by anthropogenic aerosols, *Bull. Am. Meteorol. Soc.*, *86*(12), 1795–1809, doi:10.1175/BAMS-86-12-1795.

Arimoto, R., et al. (2006), Characterization of Asian dust during ACE-Asia, *Global Planet. Change*, *52*, 23–56, doi:10.1016/j.gloplacha.2006.02.013.

Arola, A., G. Schuster, G. Myhre, S. Kazadzis, S. Dey, and S. N. Tripathi (2011), Inferring absorbing organic carbon content from AERONET data, *Atmos. Chem. Phys.*, *11*, 215–225, doi:10.5194/acp-11-215-2011.

Beegum, S. N., et al. (2008), Characteristics of spectral aerosol optical depths over India during ICARB, *J. Earth Syst. Sci.*, *117*(S1), 303–313, doi:10.1007/s12040-008-0033-y.

Bergstrom, R. W., P. B. Russell, and P. Hignett (2002), Wavelength dependence of the absorption of black carbon particles: Predictions and results from the TARFOX experiment and implications for the aerosol single scattering albedo, *J. Atmos. Sci.*, *59*, 567–577, doi:10.1175/1520-0469(2002)059<0567:WDOTAO>2.0.CO;2.

Bergstrom, R. W., P. Pilewskie, P. B. Russell, J. Redemann, T. C. Bond, P. K. Quinn, and B. Sierau (2007), Spectral absorption properties of atmospheric aerosols, *Atmos. Chem. Phys.*, *7*, 5937–5943, doi:10.5194/acp-7-5937-2007.

Chaudhry, Z., J. V. Martins, Z. Li, S.-C. Tsay, H. Chen, P. Wang, T. Wen, C. Li, and R. R. Dickerson (2007), In situ measurements of aerosol mass concentration and radiative properties in Xianghe, southeast of Beijing, *J. Geophys. Res.*, *112*, D23S90, doi:10.1029/2007JD009055.

Chinnam, N., S. Dey, S. N. Tripathi, and M. Sharma (2006), Dust events in Kanpur, northern India: Chemical evidence for source and implications to radiative forcing, *Geophys. Res. Lett.*, *33*, L08803, doi:10.1029/2005GL025278.

Chu, D. A., Y. J. Kaufman, G. Zibordi, J. D. Chern, J. Mao, C. Li, and B. N. Holben (2003), Global monitoring of air pollution over land from the Earth Observing System-Terra Moderate Resolution Imaging Spectroradiometer (MODIS), *J. Geophys. Res.*, *108*(D21), 4661, doi:10.1029/2002JD003179.

Derimian, Y., A. Karnieli, Y. J. Kaufman, M. O. Andreae, T. W. Andreae, O. Dubovik, W. Maenhaut, and I. Koren (2008), The role of iron and black carbon in aerosol light absorption, *Atmos. Chem. Phys.*, *8*, 3623–3637, doi:10.5194/acp-8-3623-2008.

Dey, S., and L. Di Girolamo (2010), A climatology of aerosol optical and microphysical properties over the Indian subcontinent from 9 years (2000–2008) of Multiangle Imaging Spectroradiometer (MISR) data, *J. Geophys. Res.*, *115*, D15204, doi:10.1029/2009JD013395.

Dey, S., and S. N. Tripathi (2007), Estimation of aerosol optical properties and radiative effects in the Ganga basin, northern India, during the wintertime, *J. Geophys. Res.*, *112*, D03203, doi:10.1029/2006JD007267.

Dey, S., S. N. Tripathi, R. P. Singh, and B. N. Holben (2004), Influence of dust storms on the aerosol optical properties over the Indo-Gangetic basin, *J. Geophys. Res.*, *109*, D20211, doi:10.1029/2004JD004924.

Dey, S., S. N. Tripathi, R. P. Singh, and B. N. Holben (2005), Seasonal variability of the aerosol parameters over Kanpur, an urban site in Indo-Gangetic basin, *Adv. Space Res.*, *36*, 778–782, doi:10.1016/j.asr.2005.06.040.

Dey, S., S. N. Tripathi, and S. K. Mishra (2008), Probable mixing state of aerosols in the Indo-Gangetic Basin, northern India, *Geophys. Res. Lett.*, *35*, L03808, doi:10.1029/2007GL032622.

Dickerson, R. R., M. O. Andreae, T. Campos, O. L. Mayol-Bracero, C. Neusuess, and D. G. Streets (2002), Analysis of black carbon and carbon monoxide observed over the Indian Ocean: Implications for emissions and photochemistry, *J. Geophys. Res.*, *107*(D19), 8017, doi:10.1029/2001JD000501.

Draxler, R. R., and G. D. Rolph (2010), HYSPLIT (HYbrid Single-Particle Lagrangian Integrated Trajectory) Model access via NOAA ARL READY Web site (http://ready.arl.noaa.gov/HYSPLIT.php), NOAA Air Resour. Lab., Silver Spring, Md.

Dubovik, O., and M. D. King (2000), A flexible inversion algorithm for retrieval of aerosol optical properties from Sun and sky radiance measurements, *J. Geophys. Res.*, *105*, 20,673–20,696, doi:10.1029/2000JD900282.

Dubovik, O., A. Smirnov, B. N. Holben, M. D. King, Y. J. Kaufman, T. F. Eck, and I. Slutsker (2000), Accuracy assessments of aerosol optical properties retrieved from AERONET Sun and sky-radiance measurements, *J. Geophys. Res.*, *105*, 9791–9806, doi:10.1029/2000JD900040.

Dubovik, O., B. N. Holben, T. F. Eck, A. Smirnov, Y. J. Kaufman, M. D. King, D. Tanre, and I. Slutsker (2002), Variability of absorption and optical properties of key aerosol types observed in worldwide locations, *J. Atmos. Sci.*, *59*, 590–608, doi:10.1175/1520-0469(2002)059<0590:VOAAOP>2.0.CO;2.

Dubovik, O., et al. (2006), Application of spheroid models to account for aerosol particle nonsphericity in remote sensing of desert dust, *J. Geophys. Res.*, *111*, D11208, doi:10.1029/2005JD006619.

Eck, T. F., B. N. Holben, J. S. Reid, O. Dubovik, A. Smirnov, N. T. O'Neill, I. Slutsker, and S. Kinne (1999), Wavelength dependence of the optical depth of biomass burning, urban, and desert dust aerosols, *J. Geophys. Res.*, *104*(D24), 31,333–31,349, doi:10.1029/1999JD900923.

Eck, T. F., B. N. Holben, J. S. Reid, N. T. O'Neill, J. S. Schafer, O. Dubovik, A. Smirnov, M. A. Yamasoe, and P. Artaxo (2003), High aerosol optical depth biomass burning events: A comparison of optical properties for

different source regions, *Geophys. Res. Lett.*, *30*(20), 2035, doi:10.1029/2003GL017861.

Eck, T. F., et al. (2005), Columnar aerosol optical properties at AERONET sites in central eastern Asia and aerosol transport to the tropical mid-Pacific, *J. Geophys. Res.*, *110*, D06202, doi:10.1029/2004JD005274.

Eck, T. F., et al. (2008), Spatial and temporal variability of column-integrated aerosol optical properties in the southern Arabian Gulf and United Arab Emirates in summer, *J. Geophys. Res.*, *113*, D01204, doi:10.1029/2007JD008944.

Eck, T. F., et al. (2009), Optical properties of boreal region biomass burning aerosols in central Alaska and seasonal variation of aerosol optical depth at an Arctic coastal site, *J. Geophys. Res.*, *114*, D11201, doi:10.1029/2008JD010870.

Eck, T. F., et al. (2010), Climatological aspects of the optical properties of fine/coarse mode aerosol mixtures, *J. Geophys. Res.*, *115*, D19205, doi:10.1029/2010JD014002.

Garland, R. M., et al. (2008), Aerosol optical properties in a rural environment near the mega-city Guangzhou, China: Implications for regional air pollution, radiative forcing and remote sensing, *Atmos. Chem. Phys.*, *8*, 5161–5186, doi:10.5194/acp-8-5161-2008.

Gautam, R., Z. Liu, R. P. Singh, and N. C. Hsu (2009), Two contrasting dust-dominant periods over India observed from MODIS and CALIPSO data, *Geophys. Res. Lett.*, *36*, L06813, doi:10.1029/2008GL036967.

Gautam, R., N. C. Hsu, and K.-M. Lau (2010), Premonsoon aerosol characterization and radiative effects over the Indo-Gangetic Plains: Implications for regional climate warming, *J. Geophys. Res.*, *115*, D17208, doi:10.1029/2010JD013819.

Giles, D. M., et al. (2010), Identifying aerosol type/mixture from aerosol absorption properties using AERONET, *Eos Trans. AGU*, *91*(26), West. Pac. Geophys. Meet. Suppl., Abstract A33D-05.

Ginoux, P., D. Garbuzov, and N. C. Hsu (2010), Identification of anthropogenic and natural dust sources using Moderate Resolution Imaging Spectroradiometer (MODIS) Deep Blue level 2 data, *J. Geophys. Res.*, *115*, D05204, doi:10.1029/2009JD012398.

Gogoi, M. M., K. Krishna Moorthy, S. S. Babu, and P. K. Bhuyan (2009), Climatology of columnar aerosol properties and the influence of synoptic conditions: First-time results from the northeastern region of India, *J. Geophys. Res.*, *114*, D08202, doi:10.1029/2008JD010765.

Guo, Z., Z. Li, J. Farquhar, A. J. Kaufman, N. Wu, C. Li, R. R. Dickerson, and P. Wang (2010), Identification of sources and formation processes of atmospheric sulfate by sulfur isotope and scanning electron microscope measurements, *J. Geophys. Res.*, *115*, D00K07, doi:10.1029/2009JD012893.

Gustafsson, Ö., M. Kruså, Z. Zencak, R. Sheesley, L. Granat, E. Engström, P. S. P. Rao, C. Leck, and H. Rodhe (2009), Brown clouds over south Asia: Biomass or fossil fuel combustion?, *Science*, *323*, doi:10.1126/science.1164857.

Hay, J. E., and P. W. Suckling (1979), An assessment of the networks for measuring and modeling solar radiation in British Columbia and adjacent areas of western Canada, *Can. Geogr.*, *23*, 222–238, doi:10.1111/j.1541-0064.1979.tb00659.x.

Holben, B. N., T. F. Eck, and R. S. Fraser (1991), Temporal and spatial variability of aerosol optical depth in the Sahel region in relation to vegetation remote sensing, *Int. J. Remote Sens.*, *12*(6), 1147–1163, doi:10.1080/01431169108929719.

Holben, B. N., et al. (1998), AERONET–A federated instrument network and data archive for aerosol characterization, *Remote Sens. Environ.*, *66*, 1–16, doi:10.1016/S0034-4257(98)00031-5.

Holben, B. N., et al. (2001), An emerging ground-based aerosol climatology: Aerosol optical depth from AERONET, *J. Geophys. Res.*, *106*(D11), 12,067–12,097, doi:10.1029/2001JD900014.

Holben, B. N., T. F. Eck, I. Slutsker, A. Smirnov, A. Sinyuk, J. Schafer, D. Giles, and O. Dubovik (2006), AERONET's Version 2.0 quality assurance criteria, in *Remote Sensing of the Atmosphere and Clouds*, edited by S.-C. Tsay et al., *Proc. SPIE*, *6408*, 64080Q, doi:10.1117/12.706524.

Hsu, N. C., S.-C. Tsay, M. D. King, and J. R. Herman (2006), Deep Blue retrievals of Asian aerosol properties during ACE-Asia, *IEEE Trans. Geosci. Remote Sens.*, *44*(11), 3180–3195, doi:10.1109/TGRS.2006.879540.

Hyer, E. J., J. S. Reid, and J. Zhang (2011), An over-land aerosol optical depth data set for data assimilation by filtering, correction, and aggregation of MODIS Collection 5 optical depth retrievals, *Atmos. Meas. Tech.*, *4*, 379–408, doi:10.5194/amt-4-379-2011.

Ichoku, C., D. A. Chu, S. Mattoo, Y. J. Kaufman, L. A. Remer, D. Tanré, I. Slutsker, and B. N. Holben (2002), A spatio-temporal approach for global validation and analysis of MODIS aerosol products, *Geophys. Res. Lett.*, *29*(12), 8006, doi:10.1029/2001GL013206.

Ichoku, C., L. A. Remer, and T. F. Eck (2005), Quantitative evaluation and intercomparison of morning and afternoon Moderate Resolution Imaging Spectroradiometer (MODIS) aerosol measurement from Terra and Aqua, *J. Geophys. Res.*, *110*, D10S03, doi:10.1029/2004JD004987.

Jacobson, M. Z. (2001), Strong radiative heating due to the mixing state of black carbon in atmospheric aerosols, *Nature*, *409*, 695–697, doi:10.1038/35055518.

Jethva, H., S. K. Satheesh, and J. Srinivasan (2005), Seasonal variability of aerosols over the Indo-Gangetic basin, *J. Geophys. Res.*, *110*, D21204, doi:10.1029/2005JD005938.

Jethva, H., S. K. Satheesh, and J. Srinivasan (2006), Systematic bias in MODIS dust aerosol retrieval at Kanpur (AERONET), Indo-Gangetic Basin, in *Remote Sensing of the Atmosphere and Clouds*, edited by S.-C. Tsay et al., *Proc. SPIE*, *6408*, 640816, doi:10.1117/12.694952.

Jethva, H., S. K. Satheesh, and J. Srinivasan (2007a), Evaluation of MODIS C004 aerosol retrievals at Kanpur, Indo-Gangetic Basin, *J. Geophys. Res.*, *112*, D14216, doi:10.1029/2006JD007929.

Jethva, H., S. K. Satheesh, and J. Srinivasan (2007b), Assessment of second-generation MODIS retrieval (Collection 005) at Kanpur, India, *Geophys. Res. Lett.*, *34*, L19802, doi:10.1029/2007GL029647.

Jethva, H., S. K. Satheesh, J. Srinvasan, and R. C. Levy (2010), Improved retrieval of aerosol size-resolved properties from moderate resolution imaging spectroradiometer over India: Role of aerosol model and surface reflectance, *J. Geophys. Res.*, *115*, D18213, doi:10.1029/2009JD013218.

Johnson, B. T., S. Christopher, J. M. Haywood, S. R. Osborne, S. McFarlane, C. Hsu, C. Salustro, and R. Kahn (2009), Measurements of aerosol properties from aircraft and ground-based remote sensing: A case-study from the Dust and Biomass-burning Experiment (DABEX), *Q. J. R. Met. Soc.*, *135*, doi:10.1002/qj.420.

Kahn, R. A., B. J. Gaitley, J. V. Martonchik, D. J. Diner, K. A. Crean, and B. Holben (2005), Multiangle Imaging Spectroradiometer (MISR) global aerosol optical depth validation based on 2 years of coincident Aerosol Robotic Network (AERONET) observations, *J. Geophys. Res.*, *110*, D10S04, doi:10.1029/2004JD004706.

Kar, J., M. N. Deeter, J. Fishman, Z. Liu, A. Omar, J. K. Creilson, C. R. Trepte, M. A. Vaughan, and D. M. Winker (2010), Wintertime pollution over the Eastern Indo-Gangetic Plains as observed from MOPITT, CALIPSO and tropospheric ozone residual data, *Atmos. Chem. Phys.*, *10*, 12,273–12,283, doi:10.5194/acp-10-12273-2010.

Kaufman, Y. J., A. Setzer, D. Ward, D. Tanré, B. N. Holben, P. Menzel, M. C. Pereira, and R. Rasmussen (1992), Biomass Burning Airborne and Spaceborne Experiment in the Amazonas (BASE-A), *J. Geophys. Res.*, *97*(D13), 14,581–14,599, doi:10.1029/92JD00275.

Kaufman, Y. J., D. Tanré, L. A. Remer, E. F. Vermote, A. Chu, and B. N. Holben (1997), Operational remote sensing of tropospheric aerosol over land from EOS moderate resolution imaging spectroradiometer, *J. Geophys. Res.*, *102*(D14), 17,051–17,067, doi:10.1029/96JD03988.

Kinne, S., T. P. Akerman, M. Shiobara, A. Uchiyama, A. J. Heymsfield, L. Miloshevich, J. Wendell, E. Eloranta, C. Purgold, and R. W. Bergstrom (1997), Cirrus cloud radiative and microphysical properties from ground observations and in situ measurements during FIRE 1991 and their application to exhibit problems in cirrus solar radiative transfer modeling, *J. Atmos. Sci.*, *54*, 2320–2344, doi:10.1175/1520-0469(1997)054<2320:CCRAMP>2.0.CO;2.

Kirchstetter, T. W., T. Novakov, and P. V. Hobbs (2004), Evidence that the spectral dependence of light absorption by aerosols is affected by organic carbon, *J. Geophys. Res.*, *109*, D21208, doi:10.1029/2004JD004999.

Kumar, S., A. K. Singh, A. K. Prasad, and R. P. Singh (2011), Variability of GPS-derived water vapor and comparison with MODIS data over the Indo-Gangetic plains, *Phys. Chem. Earth*, in press, doi:10.1016/j.pce.2010.03.040.

Lau, K.-M., and K.-M. Kim (2006), Observational relationships between aerosol and Asian monsoon rainfall, and circulation, *Geophys. Res. Lett.*, *33*, L21810, doi:10.1029/2006GL027546.

Lau, K.-M., M. K. Kim, and K.-M. Kim (2006), Asian summer monsoon anomalies induced by aerosol direct forcing: The role of the Tibetan Plateau, *Clim. Dyn.*, *26*, 855–864, doi:10.1007/s00382-006-0114-z.

Lau, K.-M., et al. (2008), The Joint Aerosol–Monsoon Experiment: A new challenge for monsoon climate research, *Bull. Am. Meteorol. Soc.*, *89*(3), 369–383, doi:10.1175/BAMS-89-3-369.

Leahy, L. V., T. L. Anderson, T. F. Eck, and R. W. Bergstrom (2007), A synthesis of single scattering albedo of biomass burning aerosol over southern Africa during SAFARI 2000, *Geophys. Res. Lett.*, *34*, L12814, doi:10.1029/2007GL029697.

Lelieveld, J., et al. (2001), The Indian Ocean Experiment: Widespread air pollution from south and southeast Asia, *Science*, *291*, 1031–1036, doi:10.1126/science.1057103.

Levy, R. C., L. A. Remer, S. Mattoo, E. F. Vermote, and Y. J. Kaufman (2007), Second-generation operational algorithm: Retrieval of aerosol properties over land from inversion of Moderate Resolution Imaging

Spectroradiometer spectral reflectance, *J. Geophys. Res.*, *112*, D13211. doi:10.1029/2006JD007811

Levy, R. C., L. A. Remer, J. V. Martins, Y. J. Kaufman, A. Plana-Fattori, J. Redemann, and B. Wenny (2005), Evaluation of the MODIS aerosol retrievals over ocean and land during CLAMS, *J. Atmos. Sci.*, *62*, 974–992, doi:10.1175/JAS3391.1.

Lewis, K., W. P. Arnott, H. Moosmüller, and C. E. Wold (2008), Strong spectral variation of biomass smoke light absorption and single scattering albedo observed with a novel dual-wavelength photoacoustic instrument, *J. Geophys. Res.*, *113*, D16203, doi:10.1029/2007JD009699.

Littmann, T. (1991), Dust storm frequency in Asia: Climatic control and variability, *Int. J. Climatol.*, *11*, 393–412, doi:10.1002/joc.3370110405.

Mani, A., O. Chacko, and S. Hariharan (1969), A study of Ångström's turbidity parameters from solar radiation measurements in India, *Tellus*, *21*, 829–843, doi:10.1111/j.2153-3490.1969.tb00489.x.

McPherson, C. J., J. A. Reagan, J. Schafer, D. Giles, R. Ferrare, J. Hair, and C. Hostetler (2010), AERONET, airborne HSRL, and CALIPSO aerosol retrievals compared and combined: A case study, *J. Geophys. Res.*, *115*, D00H21, doi:10.1029/2009JD012389.

Middleton, N. J. (1986), A geography of dust storms in south-west Asia, *J. Climatol.*, *6*, 183–196, doi:10.1002/joc.3370060207.

Misra, A., A. Jayaraman, and D. Ganguly (2008), Validation of MODIS derived aerosol optical depth over Western India, *J. Geophys. Res.*, *113*, D04203, doi:10.1029/2007JD009075.

Moorthy, K. K., and S. S. Babu (2005), Aerosol characteristics and radiative impacts over the Arabian Sea during the intermonsoon season: Results from ARMEX field campaign, *J. Atmos. Sci.*, *62*, 192–206, doi:10.1175/JAS-3378.1.

Moorthy, K. K., P. R. Nair, and B. V. K. Murthy (1989), Multiwavelength solar radiometer network and features of aerosol spectral optical depth at Trivandrum, *Indian J. Radio Space Phys.*, *18*, 194–201.

Moorthy, K. K., S. S. Babu, S. K. Satheesh, J. Srinivasan, and C. B. S. Dutt (2007), Dust absorption over the "Great Indian Desert" inferred using ground-based and satellite remote sensing, *J. Geophys. Res.*, *112*, D09206, doi:10.1029/2006JD007690.

Moorthy, K. K., S. K. Satheesh, S. S. Babu, and C. B. S. Dutt (2008), Integrated Campaign for Aerosols, gases and Radiation Budget (ICARB): An overview, *J. Earth Syst. Sci.*, *117*(S1), 243–262, doi:10.1007/s12040-008-0029-7.

Morys, M., F. M. Mims III, S. Hagerup, S. E. Anderson, A. Baker, J. Kia, and T. Walkup (2001), Design, calibration, and performance of MICROTOPS II handheld ozone monitor and Sun photometer, *J. Geophys. Res.*, *106*(D13), 14,573–14,582, doi:10.1029/2001JD900103.

Müller, D., et al. (2010), Mineral dust observed with AERONET Sun photometer, Raman lidar, and in situ instruments during SAMUM 2006: Shape-independent particle properties, *J. Geophys. Res.*, *115*, D07202, doi:10.1029/2009JD012520.

Niranjan, K., B. M. Rao, P. S. Brahmanandam, B. L. Madhavan, V. Sreekanth, and K. K. Moorthy (2005), Spatial characteristics of aerosol physical properties over the northeastern parts of peninsular India, *Ann. Geophys.*, *23*, 3219–3227, doi:10.5194/angeo-23-3219-2005.

O'Neill, N. T., T. F. Eck, B. N. Holben, A. Smirnov, O. Dubovik, and A. Royer (2001), Bimodal size distribution influences on the variation of Angstrom derivatives in spectral and optical depth space, *J. Geophys. Res.*, *106*(D9), 9787–9806, doi:10.1029/2000JD900245.

O'Neill, N. T., T. F. Eck, A. Smirnov, B. N. Holben, and S. Thulasiraman (2003), Spectral discrimination of coarse and fine mode optical depth, *J. Geophys. Res.*, *108*(D17), 4559, doi:10.1029/2002JD002975.

Orlanski, I. (1975), A rational subdivision of scales for atmospheric processes, *Bull. Am. Meteorol. Soc.*, *56*(5), 527–530.

Pinker, R. T., B. Zhang, and E. G. Dutton (2005), Do satellites detect trends in surface solar radiation?, *Science*, *308*, 850–854, doi:10.1126/science.1103159.

Prasad, A. K., and R. P. Singh (2007a), Changes in aerosol parameters during major dust storm events (2001–2005) over the Indo-Gangetic Plains using AERONET and MODIS data, *J. Geophys. Res.*, *112*, D09208, doi:10.1029/2006JD007778.

Prasad, A. K., and R. P. Singh (2007b), Comparison of MISR-MODIS aerosol optical depth over the Indo-Gangetic basin during the winter and summer seasons (2000–2005), *Remote Sens. Environ.*, *107*, 109–119, doi:10.1016/j.rse.2006.09.026.

Prasad, A. K., and R. P. Singh (2009), Validation of MODIS Terra, AIRS, NCEP/DOE AMIP-II Reanalysis-2, and AERONET Sun photometer derived integrated precipitable water vapor using ground-based GPS receivers over India, *J. Geophys. Res.*, *114*, D05107, doi:10.1029/2008JD011230.

Prasad, A. K., R. P. Singh, and M. Kafatos (2006), Influence of coal based thermal power plants on aerosol optical properties in the Indo-Gangetic basin, *Geophys. Res. Lett.*, *33*, L05805, doi:10.1029/2005GL023801.

Prasad, A. K., S. Singh, S. S. Chauhan, M. K. Srivastava, R. P. Singh, and R. Singh (2007), Aerosol radiative forcing over the Indo-Gangetic plains during major dust storms, *Atmos. Environ.*, *41*, 6289–6301, doi:10.1016/j.atmosenv.2007.03.060.

Ram, K., M. M. Sarin, and S. N. Tripathi (2010a), Inter-comparison of thermal and optical methods for determination of atmospheric black carbon and attenuation coefficient from an urban location in northern India, *Atmos. Res.*, *97*, 335–342, doi:10.1016/j.atmosres.2010.04.006.

Ram, K., M. M. Sarin, and S. N. Tripathi (2010b), A 1 year record of carbonaceous aerosols from an urban site in the Indo-Gangetic Plain: Characterization, sources, and temporal variability, *J. Geophys. Res.*, *115*, D24313, doi:10.1029/2010JD014188.

Ramanathan, V., and M. V. Ramana (2005), Persistent, widespread, and strongly absorbing haze over the Himalayan foothills and the Indo-Gangetic plains, *Pure Appl. Geophys.*, *162*, 1609–1626, doi:10.1007/s00024-005-2685-8.

Ramanathan, V., et al. (2001), Indian Ocean Experiment: An integrated analysis of the climate forcing and effects of the great Indo-Asian haze, *J. Geophys. Res.*, *106*(D22), 28,371–28,398, doi:10.1029/2001JD900133.

Ramanathan, V., et al. (2005), Atmospheric brown clouds: Impacts on South Asian climate and hydrological cycle, *Proc. Natl. Acad. Sci. U. S. A.*, *102*(15), 5326–5333, doi:10.1073/pnas.0500656102.

Remer, L. A., et al. (2005), The MODIS aerosol algorithm, products, and validation, *J. of Atmos. Sci.*, *62*, 947–973, doi:10.1175/JAS3385.1.

Remer, L. A., et al. (2008), Global aerosol climatology from the MODIS satellite sensors, *J. Geophys. Res.*, *113*, D14S07, doi:10.1029/2007JD009661.

Remer, L. A., D. Tanré, Y. J. Kaufman, R. Levy, and S. Mattoo (2009), Algorithm for remote sensing of tropospheric aerosol from MODIS: Collection 005, Revision 2, Product ID: MOD04/MYD04, *Ref. ATBD-MOD-96*, 88 pp., NASA, Greenbelt, Md. [Available online at http://modis-atmos.gsfc.nasa.gov/MOD04_L2/atbd.html.

Rolph, G. D. (2010), Real-time Environmental Applications and Display sYstem (READY), http://ready.arl.noaa.gov, NOAA Air Resour. Lab., Silver Spring, Md.

Russell, P. B., R. W. Bergstrom, Y. Shinozuka, A. D. Clarke, P. F. DeCarlo, J. L. Jimenez, J. M. Livingston, J. Redemann, O. Dubovik, and A. Strawa (2010), Absorption Ångstrom Exponent in AERONET and related data as an indicator of aerosol composition, *Atmos. Chem. Phys.*, *10*, 1155–1169, doi:10.5194/acp-10-1155-2010.

Satheesh, S. K., K. K. Moorthy, S. S. Babu, V. Vinoj, V. S. Nair, S. N. Beegum, C. B. S. Dutt, D. P. Alappattu, and P. K. Kunhikrishnan (2009), Vertical structure and horizontal gradients of aerosol extinction coefficients over coastal India inferred from airborne lidar measurements during the Integrated Campaign for Aerosol, Gases and Radiation Budget (ICARB) field campaign, *J. Geophys. Res.*, *114*, D05204, doi:10.1029/2008JD011033.

Schmid, B., et al. (2001), Comparison of columnar water-vapor measurements from solar transmittance methods, *Appl. Opt.*, *40*(12), 1886–1896, doi:10.1364/AO.40.001886.

Shaw, G. E. (1980), Transport of Asian desert aerosol to the Hawaiian Islands, *J. Appl. Meteorol.*, *19*, 1254–1259, doi:10.1175/1520-0450(1980)019<1254:TOADAT>2.0.CO;2.

Shaw, G. E. (1983), Sun photometry, *Bull. Am. Meteorol. Soc.*, *64*(1), 4–10, doi:10.1175/1520-0477(1983)064<0004:SP>2.0.CO;2.

Singh, R. P. (2010), Interactive comment on "Inferring absorbing organic carbon content from AERONET data" by A. Arola et al., *Atmos. Chem. Phys. Discuss.*, *10*, C8106, [Available online at http://www.atmos-chem-phys-discuss.net/10/C7718/2010/acpd-10-C7718-2010.pdf].

Singh, R. P., S. Dey, and B. Holben (2003), Aerosol behavior in Kanpur during Diwali festival, *Curr. Sci.*, *84*(10), 1302–1304.

Singh, R. P., S. Dey, S. N. Tripathi, V. Tare, and B. Holben (2004), Variability of aerosol parameters over Kanpur, northern India, *J. Geophys. Res.*, *109*, D23206, doi:10.1029/2004JD004966.

Singh, S., S. Nath, R. Kohli, and R. Singh (2005), Aerosols over Delhi during pre-monsoon months: Characteristics and effects on surface radiation forcing, *Geophys. Res. Lett.*, *32*, L13808, doi:10.1029/2005GL023062.

Smirnov, A., B. N. Holben, T. F. Eck, O. Dubovik, and I. Slutsker (2000), Cloud-screening and quality control algorithms for the AERONET database, *Remote Sens. Environ.*, *73*, 337–349, doi:10.1016/S0034-4257(00)00109-7.

Smirnov, A., B. N. Holben, A. Lyapustin, I. Slutsker, and T. F. Eck (2004), AERONET processing algorithms refinement, paper presented at AERONET Workshop, El Arenosillo, Spain, 10–14 May.

Smirnov, A., et al. (2009), Maritime Aerosol Network as a component of Aerosol Robotic Network, *J. Geophys. Res.*, *114*, D06204, doi:10.1029/2008JD011257.

Toledano, C., et al. (2011), Optical properties of aerosol mixtures derived from sun-sky radiometry during SAMUM-2, *Tellus, Ser. B*, *63*, 635–648, doi:10.1111/j.1600-0889.2011.00573.x.

Tripathi, S. N., S. Dey, A. Chandel, S. Srivastava, R. P. Singh, and B. N. Holben (2005a), Comparison of MODIS and AERONET derived aerosol optical depth over the Ganga Basin, India, *Ann. Geophys.*, *23*, 1093–1101, doi:10.5194/angeo-23-1093-2005.

Tripathi, S. N., S. Dey, V. Tare, and S. K. Satheesh (2005b), Aerosol black carbon radiative forcing at an industrial city in northern India, *Geophys. Res. Lett.*, *32*, L08802, doi:10.1029/2005GL022515.

Vaughan, M. A., S. A. Young, D. M. Winker, K. A. Powell, A. H. Omar, Z. Liu, Y. Hu, and C. A. Hostetler (2004), Fully automated analysis of space-based lidar data: An overview of the CALIPSO retrieval algorithms and data products, in Laser Radar Techniques for Atmospheric Sensing, edited by U. N. Singh, *Proc. SPIE*, *5575*, 16–30, doi:10.1117/12.572024.

R. R. Dickerson, Department of Atmospheric and Oceanic Science, The University of Maryland, College Park, MD 20742, USA.

T. F. Eck, Universities Space Research Association, 10211 Wincopin Circle, Ste. 500, Columbia, MD 21044-3432, USA.

D. M. Giles, I. Slutsker, A. Sinyuk, and J. S. Schafer, Sigma Space Corporation, Code 614.4, NASA/GSFC, Greenbelt, MD 20771, USA. (David.M.Giles@nasa.gov)

B. N. Holben, Biospheric Sciences Branch, NASA/GSFC, Code 614.4, Greenbelt, MD 20771, USA.

S. Mattoo, Science Systems and Applications, Inc., Code 613.2, NASA/GSFC, Greenbelt, MD 20771, USA.

R. P. Singh, School of Earth and Environmental Sciences, Schmid College of Science, Chapman University, Hashinger Science Center 219, One University Dr., Orange, CA 92866, USA.

A. M. Thompson, Department of Meteorology, College of Earth and Mineral Sciences, The Pennsylvania State University, 510 Walker Bldg., University Park, PA 16802, USA.

S. N. Tripathi, Indian Institute of Technology Kanpur, Department of Civil Engineering, 306 Faculty Bldg., Uttar Pradesh, Kanpur 208016, India.

S.-H. Wang, Department of Atmospheric Sciences, National Central University, No. 300 Jhongda Rd., Jhongli City, Taoyuan County 32001, Taiwan.